GA-A24648

ADVANCED FUSION TECHNOLOGY RESEARCH AND DEVELOPMENT

ANNUAL REPORT TO THE U.S. DEPARTMENT OF ENERGY

OCTOBER 1, 2002 THROUGH SEPTEMBER 30, 2003

by

PROJECT STAFF

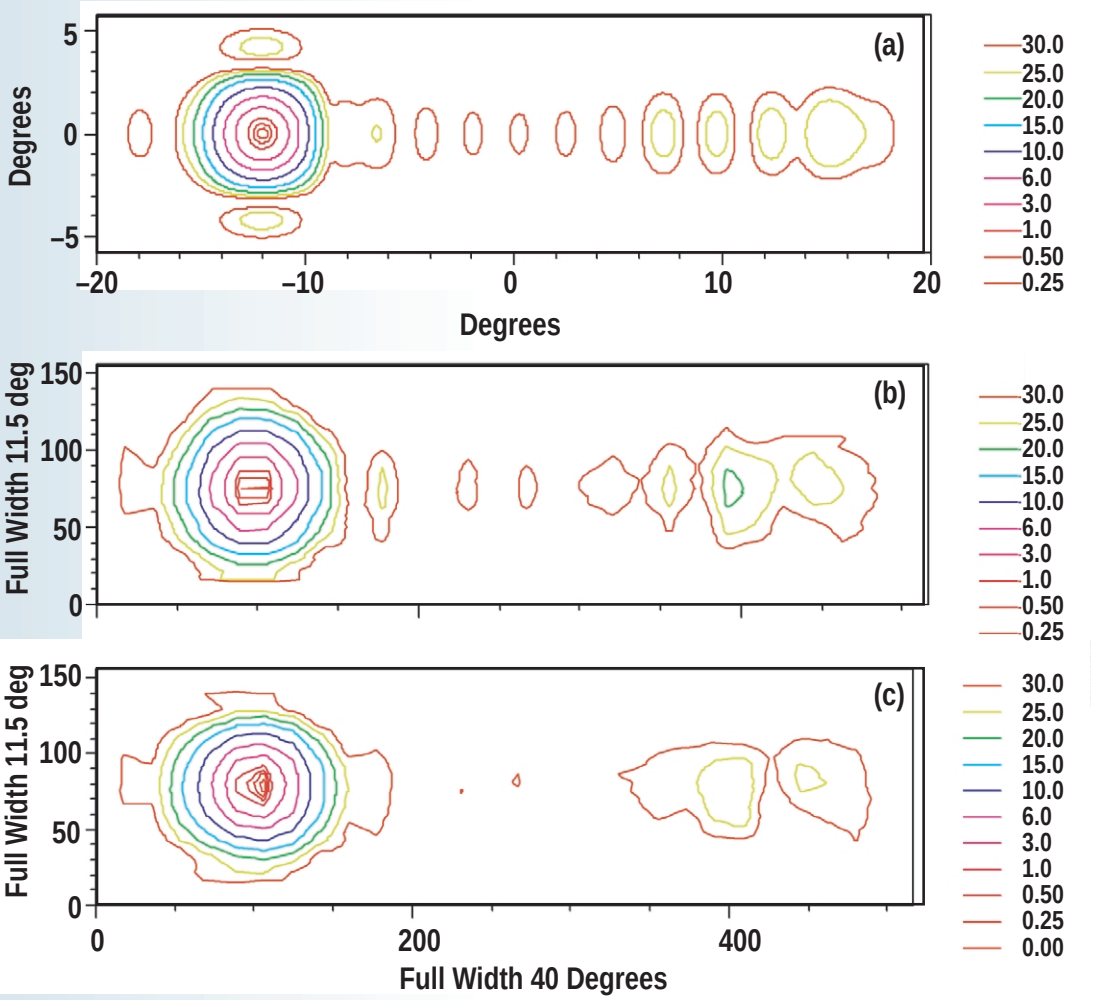

JUNE 2004

GENERAL ATOMICS

GA–A24648

ADVANCED FUSION TECHNOLOGY RESEARCH AND DEVELOPMENT

ANNUAL REPORT TO THE U.S. DEPARTMENT OF ENERGY

OCTOBER 1, 2002 THROUGH SEPTEMBER 30, 2003

by

PROJECT STAFF

Work prepared under
Department of Energy
Contract No. DE-AC03-98ER54411

GENERAL ATOMICS PROJECT 30007
DATE PUBLISHED: JUNE 2004

DISCLAIMER

This report has been reproduced
directly from the best available copy

Available to DOE and DOE contractors from the
Office of Scientific and Technical Information
P.O. Box 62
Oak Ridge, TN 37831
Prices available from (615) 576-8401,
FTS 626-8401

Available to the public from the
National Technical Information Service
U.S. Department of Commerce
5285 Port Royal Road
Springfield, VA 22161

Cover Art: Calculated radiation pattern at a steering angle of –12° (top curve) and the measured patterns for E field in the perpendicular and parallel directions (bottom two curves). See Section 9.2.

TABLE OF CONTENTS

LIST OF FIGURES

LIST OF TABLES

1. INTRODUCTION

The General Atomics (GA) Advanced Fusion Technology program seeks to advance the knowledge base needed for next-generation fusion experiments and for reaching the ultimate goal of an economical and environmentally attractive fusion energy source. To achieve this objective, GA conducts fusion systems design studies to evaluate the technologies needed for next-step experiments and power plants, as well as research to develop basic and applied knowledge about these technologies. GA's Advanced Fusion Technology program derives from, and draws on, the physics and engineering expertise gained through many years of experience in designing, building, and operating plasma physics experiments. Our technology development activities take full advantage of the GA DIII–D program, the DIII–D facility, the Inertial Confinement Fusion (ICF) program and the ICF Target Fabrication facility.

The sections within this report summarize GA's FY03 work in the areas of Fusion Power Plant Studies (ARIES, Section 2), Inertial Fusion Energy Chamber Analysis (Section 3), Inertial Fusion Energy Target Supply System (Section 4), Next Step Fusion Design (Section 5), Advanced Liquid Plasma Facing Surfaces (ALPS, Section 6), Advanced Power Extraction Study (APEX, Section 7), Plasma-Facing Components (DiMES, Section 8) and RF Technology (Section 9). Our work in these areas continues to address many of the issues that must be resolved for the successful construction and operation of next-generation experiments and, ultimately, the development of safe, reliable, economic fusion power plants.

Our work was supported by the Office of Fusion Energy Sciences, U.S. Department of Energy.

2. FUSION POWER PLANT STUDIES (ARIES-MFE)

2.1. EVALUATION OF NUMERICAL EQUILIBRIUM AND STABILITY TOOLS FOR COMPACT STELLARATORS

The initial phase of the project was to evaluate the current state of the numerical tools that are available for calculating the equilibria and stability of Compact Stellarators. The main conclusions from this work can be summarized as follows:

1. The situation is adequate for numerical equilibrium tools, with the VMEC code for accurate and fast equilibrium calculations suitable for stability analysis, and the HINST and PIES codes for evaluating the "realizability" of the equilibria.

   The major deficiency is the lack of a 3-D Stellarator equilibrium fitting code analogous to EFIT for 2-D equilibria. This is not needed for the ARIES Compact Stellarator design, but it will be essential for future interpretation of Compact Stellarator experiments.

2. For global ideal linear stability tools, the situation is almost adequate since there are two well-developed codes available — TERPSICHORE and CAS-3D.

   There are, however, two major deficiencies. A completely robust, vacuum formulation does not exist even though TERPSICHORE has a working vacuum boundary condition for some cases. Second, there is no linear stability code capable of handling islands or ergodic regions. This is a problem for Stellarator research in general.

3. For linear resistive stability, the situation is inadequate. The SPECTOR-3D code is intended to fill this void but is still under development. Nevertheless, there is no other comparable code and SPECTOR-3D is used for analysis of the H-1 Heliac.

2.2. EQUILIBRIUM AND STABILITY FOR COMPACT STELLARATORS

2.2.1. Porting of Terpsichore Ideal MHD Stability Code to Local Platforms

In collaboration with the original author, W.A. Cooper of CRPP in Lausanne, Switzerland, the TERPSICHORE 3-D ideal MHD stability code was successfully ported to the local Lohan1 Linux workstation at General Atomics (GA) and reproduced benchmark results for LHD and QHS. A three-field-period Compact Stellarator equilibrium, scaled up from NCSX, was provided by Long-Poe Ku of PPPL for stability testing.

2.2.2. Equilibrium and Stability Analysis

As a first step to constructing a sequence of equilibria with increasing β and searching for the stability limit, the three-period scaled-up NCSX equilibrium was reproduced using the GA version of the VMEC code. This particular equilibrium has $\langle\beta\rangle = 4.1\%$ and A = 4.47. The stability results for this equilibrium are, unfortunately, restricted to a range of moderately placed external conformal conducting walls between 1.7 and 2.7 times the minor radius of the plasma. For the wall in this range, the plasma is stable with an oscillation frequency normalized to the toroidal Alfvén time of 0.9088×10^{-2}.

A sequence of higher β equilibria was then constructed in the same manner using the GA version of VMEC. The volume, average major radius, average minor radius, and vacuum toroidal field were held fixed as β was increased through uniformly scaling the pressure profile. Also, the shape of the outer plasma boundary was also held fixed. The major equilibrium change is an outward shift in the magnetic axis as β increases.

This sequence was then tested for ideal stability at the intermediate wall positions where the TERPSICHORE code works. For the three field-period stellarator, mode coupling is confined to a single mode family represented by n = 1. Table 1 shows the stability results — the squared growth rate γ^2 versus the equilibrium β for the most unstable mode within the mode family. The growth rates are normalized to a toroidal Alfvén transit time. Positive γ^2 implies the plasma is stable; negative γ^2 implies instability.

TABLE 1
SQUARED GROWTH RATE FOR VMEC FIXED BOUNDARY EQUILIBRIUM SEQUENCE WITH INCREASING β AT VARYING INTERMEDIATE WALL POSITIONS

β/Wall Position (%)	1.7	2.0	2.5
4.1	$+8.65 \times 10^{-5}$	$+8.65 \times 10^{-5}$	$+8.65 \times 10^{-5}$
5.7	$+1.81 \times 10^{-4}$	$+1.81 \times 10^{-4}$	$+1.81 \times 10^{-4}$
7.0	-8.66×10^{-4}	-9.47×10^{-3}	-1.62×10^{-2}
8.3	-7.25×10^{-2}	-7.75×10^{-2}	-8.06×10^{-2}

This suggests a β limit ≈ 6% for this configuration with an intermediate wall of order twice minor radius. Numerical convergence studies with mesh size are needed to confirm this limit but are not expected to drastically change this result. Since the n = 1 toroidal mode family is the only one present for a three-field-period device, this should provide the actual β limit.

2.3. DETERMINATION OF THE FAILURE IN VACUUM CALCULATION IN TERPSICHORE

The direct cause of the failures in the TERPSICHORE vacuum calculation was analyzed and determined in collaboration with A.W. Cooper. With increasing a_w, the outboard wall begins to move inward slightly at some toroidal planes in which the plasma is bean shaped and up-down symmetric; when $a_w > 2.7$, the wall then cuts the plasma-vacuum interface at a point on the outboard mid-plane. When $a_w < 1.7$, on the other hand, the wall approaches the inboard plasma surface at one toroidal plane and the vacuum calculation fails due to the logarithmic singularity in the solution as the plasma-wall distance locally vanishes.

This is a well-known problem with the TERPSICHORE code and is the source of the comment in Section 1.0 concerning the lack of a 3-D ideal MHD stability code that robustly handles the vacuum. This will take a significant effort that is beyond the scope of the present contract to resolve.

2.4. ISSUES: MEANING OF STABILITY LIMITS IN STELLARATORS

In the course of the numerical equilibrium and stability tool evaluation, it became clear that there is an issue regarding the meaning of ideal MHD stability limits in stellarators. W7-AS and LHD have exceeded predicted β limits by significant margins; the local limits have been exceeded by factors of up to two. Stellarator designs that are based on optimizing against linear ideal MHD stability are therefore questionable. This issue needs continuing investigation within the stellarator community. Alan Turnbull arranged for a special discussion of the relevance of MHD stability calculations to the large stellarator experiments in the National Stellarator Theory Teleconference series. In the June teleconference, M. Zarnstorff presented results from W7-AS and LHD. In the July Teleconference, Alan Turnbull and Paul Garabedian presented their views.

While there is not yet closure, there are two possible resolutions based on experience with tokamak stability limits. First, the equilibria in the discharges are not necessarily those used in the stability predictions. Experience with tokamaks has shown that the ι (or q) profile is not necessarily what "reasonable" theoretical arguments suggest it should be. Routine measurements of the pressure and ι profiles at finite β, like those in large tokamaks, are needed to pin down the apparent violation of predicted stability limits. Even the assumption that the surfaces are nested may not be the case in the stellarator discharges; it may be necessary to use free boundary non-nested equilibria and/or nonlinear stability studies to obtain meaningful predictions.

Second, the nonlinear consequences of linearly unstable ideal modes need to be understood. A distinction should be made between local and global ideal MHD β limits. Local limits can be dispensed with, since predictions from the infinite toroidal mode number, *n*, local ideal limit appear to be misleading; global stability calculations are much closer to experimental stability limits and local MHD stability criteria appear to be irrelevant. For

linearly unstable global modes, the nonlinear consequences need to be examined on a case-by-case basis. It is widely recognized that some predicted ideal limits in tokamaks can be violated, but the nonlinear consequences are not serious in that they do not directly lead to disruptions. This is fairly well understood on an intuitive level in tokamaks, but the same understanding is not yet available for stellarators. One needs to know which ones are serious and which are not.

One approach to evaluating nonlinear stability, while avoiding the time consuming nonlinear MHD stability calculations, is to treat the problem as one of bifurcation of MHD equilibria. The existence of a nested flux surface equilibrium can be considered as either an equilibrium problem or a stability problem; unstable equilibria with nested surfaces will evolve to a nearby state of non-nested surfaces with lower energy, if it is physically possible. Therefore, the VMEC, PIES, and HINST equilibrium codes can guarantee some degree of stability since any equilibrium computed under certain constraints must be stable, unless those numerically imposed constraints can be avoided by a physically valid motion. In this sense, PIES and HINST can guarantee some stability for equilibria with islands or ergodic regions. However, the guarantee is subject to important caveats since it is not always clear what constraints are actually imposed in any code.

Alternatively, the NSTAB equilibrium and stability code, which exploits this approach, can be used. This code applies the MHD variational principle to compute weak solutions of the conservation form of the dynamical equations. The code computes fixed boundary 3-D equilibria and nonlinear stability, which is tested by applying a mountain-pass theorem with a search for multiple or bifurcated equilibria. The code utilizes a finite difference scheme that captures discontinuities with unusually fine resolution; the discontinuities represent islands.

2.5. SUMMARY

The technical progress toward the planned goals is summarized in Table 2. The completed items are shown in bold type. The sixth item is to be completed in FY04. Also, the last two items are italicized; these are outside the limited scope of the present contract but are listed as items that will inevitably need to be done, as elaborated in Section 2.4 above.

Resolving the questions raised in Section 2.4 will require routine measurements of the pressure and ι profiles at finite β, like those in large tokamaks, and a heuristic understanding of the expected consequences of predicted linear instabilities through routine comparisons of the predictions with nonlinear predictions and observations. Non-ideal contributions also need to be explored when ideal predictions fail.

TABLE 2
PROGRESS OCTOBER 1, 2002 TO SEPTEMBER 30, 2003

Task	Status	Comments
Evaluate status of numerical equilibrium and stability tools for compact stellarators	Completed January 2003	Status as of January 2003 summarized in January 2003 Team Meeting with outstanding issues identified
Port terpsichore	Completed February 2003	Terpsichore now running on GA Linux system (Lohan1)
		Benchmarked for LHD and QHS cases (with W.A. Cooper)
Obtain base VMEC equilibrium	Completed March 2003	Obtained scaled NCSX equilibrium from PPPL to use as starting point (with Long-Poe Ku)
Stability calculation using terpsichore	Completed June 2003	Rewritten interface between VMEC and Terpsichore to use PPPL and GA VMEC and CRPP Terpsichore versions
Modify VMEC equilibrium	Completed September 2003	Reproduced PPPL scaled NCSX equilibrium using GA VMEC version and constructed equilibrium sequence with increasing β
Check stability and robustness	In Progress September 2003	Stability calculations completed for equilibrium sequence with increasing β for varying wall positions
		Sensitivity and convergence studies not fully completed
Free boundary equilibrium from PIES	Not Done	This should be done in the long run but is beyond present resources
Iterate equilibrium and stability	Not Done	This should be done in the long run but is beyond present resources

3. FUSION POWER PLANT STUDIES (ARIES-IFE)

3.1. BACKGROUND

The ARIES Program is a multi-institutional activity to explore and develop the commercial potential of fusion as a future energy source. This is accomplished through integrated systems studies of both MFE and IFE power plant concepts. Here we describe our work on the IFE portion of the study. Our task was to provide target injection and target fabrication input to the ARIES-IFE integrated system studies.

We participated in the ARIES IFE meetings listed in the following sections as well as monthly conference calls. The ARIES study emphasized the examination of the wetted wall chamber through the early part of the FY03 reporting period, and moved on to the examination of the thick, liquid wall design later in the year. We provided updates on target fabrication and injection research and participated in the development of target and chamber design guidelines as they affect target fabrication and injection. In this regard, we often brought results to ARIES meetings and reported ongoing work regardless of funding source.

3.2. HOHLRAUM MATERIALS SELECTION

Our primary ARIES task was to systematically evaluate the issues associated with the selection of hohlraum materials for the Heavy Ion Fusion (HIF) target (Fig. 1), and to optimize the materials from the view of a viable power plant system. The materials selected and used in indirect-drive targets affect many aspects of an IFE power plant system. To choose a list of reasonable target materials, we considered the effect of these materials on:

- Cost and complexity (even feasibility) of target fabrication
- Target strength for injecting the targets
- Target physics for target gain
- Methods of extracting materials from the reaction chamber
- Radioactive inventory of materials
- Cost of target materials and
- Ability to recycle materials

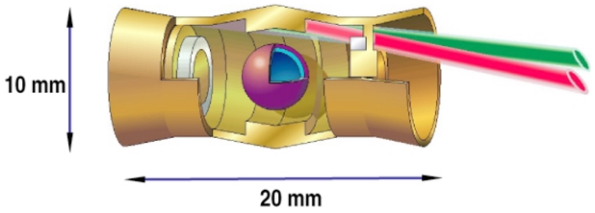

Fig. 1. LLNL close coupled heavy ion fusion target [1].

Using selection criteria, we eliminated most elements from further consideration. We found a short list of reasonable material choices, each with distinct advantages and disadvantages. Tungsten is found to be a leading material choice and a method for removing tungsten from Flibe in a liquid wall chamber was investigated.

3.2.1. Materials Selection

Jeff Latkowski [2] and Ralph Moir [3] have considered criteria by which some materials may be judged acceptable or unacceptable for indirect drive target fabrication. We used these considerations as a starting point for our study.

Latkowski considered the induced radioactivity of materials that have undergone radiation exposure from being part of a 500 MJ IFE target. The radioactivity after one week was considered for recycling purposes. Radioactivity levels at the end of plant life were evaluated to see if the material could be disposed of as low-level waste. Latkowski assigned a "hands-on" recycling dose limit of 25 μSv/h (based on a 50 mSv/yr worker dose) and a remote recycling limit of 100 mSv/h (which may be too conservative). After one week only Be, B, C, N, O, F, Cl, and Ar met the hands-on recycling dose rate limit. Ne, S, P, and K did not meet the hands-on limit, but these elements met the remote recycling limit after one week. Since we expect that remote recycling will increase target fabrication costs by an order of magnitude, we will reject recycling for materials not meeting the hands-on criteria. The one-week criteria may be too restrictive and could be revisited.

There are many more materials that could be ultimately disposed of as low-level waste. Those that could meet shallow land burial requirements in unlimited quantities are Be, B, C, O, F, Ne, Na, Mg, Si, S, P, Sc, Ti, V, Cr, Mn, Fe, Co, Cu, Zn, Ga, Ge, As, Rb, Sr, Y, In, Sn, Sb, I, Xe, Cs, Ba, La, Ce, Pr, Nd, Yb, Lu, Hf, Ta, W, Au, Hg, and Pb. Levels of the following materials in excess of parts per 1000 may be problematic: N, Al, Cl, Ar, K, Ca, Ni, Se, Br, Kr, Ru, Rh, pd, Cd, Te, Sm, Dy, Er, Tm, Re, Os, and Pt. Levels of the following elements in excess of parts per million may be problematic: Nb, Mo, Ag, Eu, Gd, Tb, Ho, Ir, and Bi. We intend to eliminate those materials that will not qualify for shallow land burial.

Moir [3] considered all high atomic number elements for hohlraum walls and suggested many that could be eliminated. Only 14 high atomic number elements (Pb, Tl, Hg, W, Ta, Hf, Lu, Yb, Nd, Pr, Ce, La, Cs, and Xe) met Moir's requirements and the shallow land burial

requirement. We deleted half of the original 14 elements due to cost, extreme chemical toxicity, difficulty of fabrication and cost/difficulty of separation from Flibe, leaving the following 7 candidates:

W, Yb, Nd, Pr, Ce, La (in group A – high atomic number) and Pb (in group B – very high atomic number).

Tungsten is the least costly of the above group A elements. A combination of high and very high atomic number elements usually improve target energetics by limiting the energy that escapes through the hohlraum walls [1]. W and Pb/W are preferred materials for hohlraum wall materials, having the following advantages and disadvantages.

1. **Pb/W** (70/30 wt %):
   - — Advantage = Small energy penalty: Ewall/Ewall-AuGd=1.08 → additional ~M$60 driver cost and ~ 0.8 mills/kWh COE over AuGd, industrial materials with low/moderate-cost (only~M$0.622 per FPY=1.1 m^3),both solid at RT, amenable to LCVD, Pb liquid → separable by centrifugation and/or settling. W precipitates in Flibe → separable by centrifugation, filtering, or settling.
   - — Disadvantage = Two materials, both may settle in Flibe loop, Pb is moderately toxic and produces mixed waste. Flibe loop must be designed to resist corrosion by Pb. W may plate on to power plant surfaces and clog small openings.
2. **W**:
   - — Advantage = Industrial, moderate-cost, single material, solid at RT, non-toxic, amenable to LCVD, precipitates in Flibe → separable by centrifugation filtering, or settling.
   - — Disadvantage = Ewall/Ewall-AuGd=1.25 → additional ~M$ 130 driver cost and ~1.8 mills/kWh COE over AuGd, material cost per FPY ~ 3.7 times Pb/W (70/30)(~M$2.310 per FPY=1.1 m^3), may settle in Flibe loop. W may plate on to plate on to power plant surfaces and clog small openings.

We developed a concept to minimize the amount of tungsten that can plate on to plant surfaces, thereby keep it from clogging spray nozzles, especially in the tritium vacuum disengager. We recognized that plating of carbon on piping and equipment surfaces could also occur, and that carbon removal would then also be necessary. The proposed approach is to seed the Flibe with powdered tungsten carbide and powdered tungsten. Seeding the Flibe with fine, recycled tungsten-carbide powder creates high surface-area nucleating sites on which the individual tungsten carbide molecules deposit — as opposed to deposition on the FLIBE loop equipment and piping surfaces. This seeding nucleation technique is a basic principle used on a mass production basis in the crystallization industry. As the tungsten-carbide particles grow, they are removed from the system with some combination of

hydroclones, centrifuges, screens, strainers, filters or settling chambers. A small fraction of the removed particles are finely ground to allow recycle as seed material.

Seed particles can be disbursed in the Flibe using a high sheer mixer (Fig. 2). Our calculations show that a 0.12% volume fraction of Tungsten powder (1.5 m^3 in the HYLIFE II plant) with average diameter 1.5 microns, could provide 100 times the surface area of the power plant surfaces and reduce growth rate on surfaces to 1 micron per year. With this amount of particles in the Flibe, the diffusion time for atoms to diffuse to a particle is about 0.7 s. Since loop transit time is about 15 s, a further reduction of the particle concentration should be possible without causing excessive plating of material on small orifices. Adding about 2 kg/day of 0.5 micron-diameter seed particles is sufficient to remove 150 kg/day. The particles will be filtered from a small (5 liter/min) slipstream.

Further study is necessary to verify that the particles will not agglomerate or cause significant wear on piping or screen surfaces.

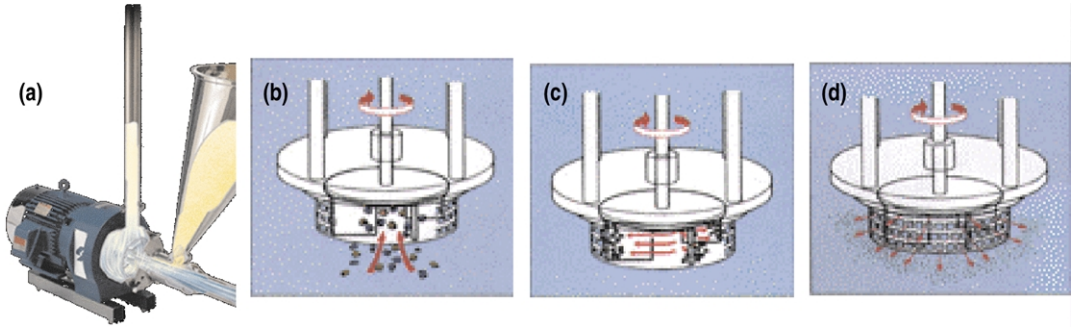

Fig. 2. (a) Silverson high-shear mixer operation. (b) Powder and fluid drawn in. (c) Powder and fluid thrown outward and milled with high speed blades. (d) Mixture is ejected with high shear.

3.3. CONFERENCES AND MEETINGS

ARIES project meeting on October 2–4, 2002, Princeton, NJ. Presented “Indirect-drive Target Aerosol Limits, Foam Mechanical Properties, and Target Injection Accuracy”.

ARIES project meeting on January 8–10, 2003, San Diego, CA. Presented “Indirect Drive Target Materials Selection and Costing Studies”.

ARIES town meeting on liquid wall chamber dynamics on May 5–6, 2003, Livermore, CA. Presented “Indirect Drive Target Materials Selection and Costing Studies”.

ARIES project meeting on May 6–7, 2003, Livermore, CA. Presented “Summary of Target Factory Labor Assumptions” and “Mitigation of Target Assembly Step Failure”.

ARIES project meeting on September 3–4, 2003, Atlanta, GA. Presented “Target Materials Selection and Removal of WC from Flibe”.

4. INERTIAL FUSION ENERGY (IFE) CHAMBER ANALYSIS

4.1. BACKGROUND

The Inertial Fusion Energy (IFE) Chamber Analysis project works to assist the national fusion program in the identification, analysis and evaluation of critical issues for both IFE and Magnetic Fusion Energy (MFE). The program enhances the synergism in research and development planning and execution for chamber technology issues common to IFE and MFE. It also facilitates technical collaboration on innovative chamber technology concepts among scientists in the United States and other countries.

Chamber technology components for IFE and MFE have some unique as well as common issues. Liquid walls, for example, have long been proposed in IFE but are recently being explored for use in MFE under the APEX and ALPS projects.

4.2. VAPOR CONDENSATION EXPERIMENTS

FY03 research work for the IFE Chamber Analysis project focused on experimental study of vapor condensation for the assessment of chamber clearing in IFE systems that include a liquid protection scheme. The HYLIFE-II chamber concept is considered as reference design, but the study is relevant to all applications of liquid walls in IFE chambers. In the IFE chamber, super heated vapor is generated from the absorption of the energy released in the fusion pulse by the protective liquid. Vacuum conditions must be restored after each fusion pulse to efficiently couple the energy drivers with the target. Since economic assessment of energy generation requires consideration of repetition rates of a few pulses per second, the study of the transient condensation of vapors becomes a key issue for the feasibility of liquid walls protection schemes in IFE systems.

This work investigated the fundamental mechanism responsible for chamber clearing: the condensation of superheated vapor in contact with a liquid surface. Since chemical processes such as recombination and diffusion play an important role in determining condensation rates, it is necessary to investigate prototypical materials if conditions relevant to IFE studies are to be met. The vapors investigated are fluorine compounds. A polymeric chain of fluorine and carbon molecules (Teflon) was first used to test the facility, followed by pure lithium fluoride and finally the prototypical molten salt FLiBe.

In IFE chambers, superheated vapor is generated by absorption of x-ray flux emerging from the nuclear explosion by the surfaces of the protective liquid structure. In the facility used for this work, the vapor is generated by a high-current, pulsed, electrical discharge.

Design of the electrical network and the high-voltage safety assessment of the facility was performed in 2002 through a collaboration between GA and the University of California, Los Angeles (UCLA) Fusion Science and Technology Center.

Experiments are designed to scale the initial density of the generated vapor, the initial energy density and the surface area available for condensation, in order to generate data relevant to the HYLIFE chamber conditions. Clearing rates are evaluated from the measured pressure history inside the scaled chamber. The main objective of this work is then to measure the pressure decay, particularly the time needed for the pressure to drop from a prototypical initial peak to the low pressure level required in the IFE chamber design. Other diagnostic tools are also employed to further characterize the condensation process. The composition of the gas after the discharge is investigated with mass spectroscopy. SEM analysis of material condensed on collecting plates is used to investigate the issues of in-flight volumetric condensation as well as the effect of the vapor velocity direction on the condensation rate.

4.3. EXPERIMENTAL RESULTS

The main result achieved in 2003 was the experimental measurement of the condensation rate of excited FLiBe vapors in conditions relevant to IFE chamber design. The key engineering contribution allowing for achievement of this result was the design of the excited vapor source. The excited vapor source was based on direct vaporization of a liquid pool of FLiBe, which also acts as the anode of the high-current arc responsible for vapor generation. The data show that the pressure decay is exponential, with a decay time constant of 6.58 ms. Accordingly, the clearing period for the reference IFE power plant is 60 ms. The conclusion is that condensation rates are sufficiently fast to allow the required repetition rates, and that the feasibility issue involved with the use of FLiBe lies in the control of the impurity dissolved in the salt.

Another original contribution is the finding that the condensation of FLiBe vapors with high kinetic energy is inhibited on surfaces that are normal to the main flow direction. It is thought that this is caused by the sharp increase in temperature due to gas stagnation near the condensing surface.

In parallel, modeling of vapor condensation has been developed, with a focus on coupling existing numerical tools that are used to simulate vapor dynamics with a module that accounts for condensation at the boundaries. The Tsunami code developed at UC Berkeley was chosen for this purpose. Tsunami was successfully coupled with the condensation subroutine to account for mass transfer at the boundaries of the numerical domain. The numerical tool was applied to the conditions encountered in the FLiBe vapor condensation experiments at UCLA. Numerical results show that the experimental conditions can be effectively simulated. The discrepancies with the experimental data were analyzed based on the code limitations and further development of the model suggested.

5. INERTIAL FUSION ENERGY (IFE) TARGET SUPPLY SYSTEM

5.1. BACKGROUND

The overall purpose of this task is to address issues associated with the target supply system for a future inertial fusion energy (IFE) power plant. This includes the major areas of target fabrication,[1] injection, and tracking. The long-term work scope for this task is to address the following issues:

- Ability to economically fabricate, fill, and layer targets that meet IFE requirements.
- Ability of targets to withstand acceleration into the reaction chamber.
- Ability of targets to survive in the chamber environment (heating due to radiation and gases).
- Accuracy and repeatability of target injection.
- Ability to accurately track targets.

5.2. FY03 SCOPE AND OBJECTIVES

This work is for indirect-drive targets, or tasks that are generic to either indirect- or direct-drive targets. Work on laser-driven, direct-drive target fabrication and injection is being accomplished under separate funding from the Naval Research Laboratory.

Major accomplishments under this scope of work:

- Completion of a cost estimate with potential mass-production methods for producing indirect drive targets.
- Hosting of the US/Japan target fabrication and injection workshop.
- Coordination of the review process for the papers from the IAEA technical meeting on the technology of fusion energy.
- Performance of ANSYS calculations to determine stress and strain in targets accelerated in a rifled barrel.

[1]GA is supporting LANL, which is the lead lab for target fabrication.

5.3. TARGET FABRICATION

An indirect-drive target (Fig. 3) consists of a fuel capsule within a cylindrical metal container known as a hohlraum, which converts the incident driver energy into x-rays to implode the capsule. The Target Fabrication Facility (TFF) of an IFE power plant must supply about 500,000 targets per day. The feasibility of developing successful fabrication and injection methodologies at the low cost required for energy production (about $0.25/target, approximately 10^4 less than current costs) is a critical issue for inertial fusion.

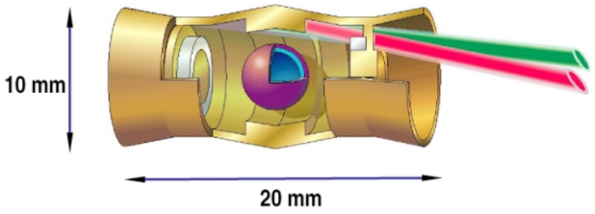

Capsule Material	CH
Capsule Diameter	~4.6 mm
Capsule Wall Thickness	250 μm
Out-of-Round	<1% of radius
Non-Concentricity	<1% of wall thickness
Shell Surface Finish	20–200 nm RMS
Ice Surface Finish	1–10 μm RMS
Temperature at shot	~16 – 18.5K
Positioning in chamber	less than ± 1–5 mm
Alignment with beams	<200 μm

Fig. 3. Reference target design and approximate specifications.

Statistical process control will be employed along with rapid “quick-check” methods to ensure the validity of each target prior to injection. This eliminates the major costs due to individual characterization of current-day targets. Ongoing target technology development programs will result in increased product yields and, finally, “nth-of-a-kind” plants will naturally operate with larger batch sizes. These factors will all contribute to major cost reductions for mass production of targets.

We completed a chemical engineering analysis of an “nth-of-a-kind” target fabrication facility for the HIF target. A preliminary target fabrication facility layout is shown in Fig. 4. There are many steps leading to a filled, layered target ready for injection. First, the highly spherical and concentric capsule must be manufactured. We anticipate that the capsules will be formed by micro-encapsulation. The capsules will be cured in rotary contactors and vacuum dried. The capsule must be filled with a mixture of deuterium and tritium (DT) as the fusion fuel. DT is permeated through the capsule wall in a high-pressure cell. Once the capsule internal density reaches the required value, the cell is cooled down to approximately 20 K to condense the fuel and reduce the internal pressure sufficiently to allow removal of

the excess DT outside the capsule. The filled capsules, which now must be handled cryogenically, are then placed in an extremely isothermal temperature environment to redistribute the DT into a highly uniform layer on the inner surface of the capsule (a process called “layering”). One method to achieve the required isothermal environment is through use of a cryogenic fluidized bed, which provides a highly uniform time-averaged surface temperature for the capsule. Once layered, the capsule is removed from the fluidized bed and quickly placed into the hohlraum for injection into the target chamber.

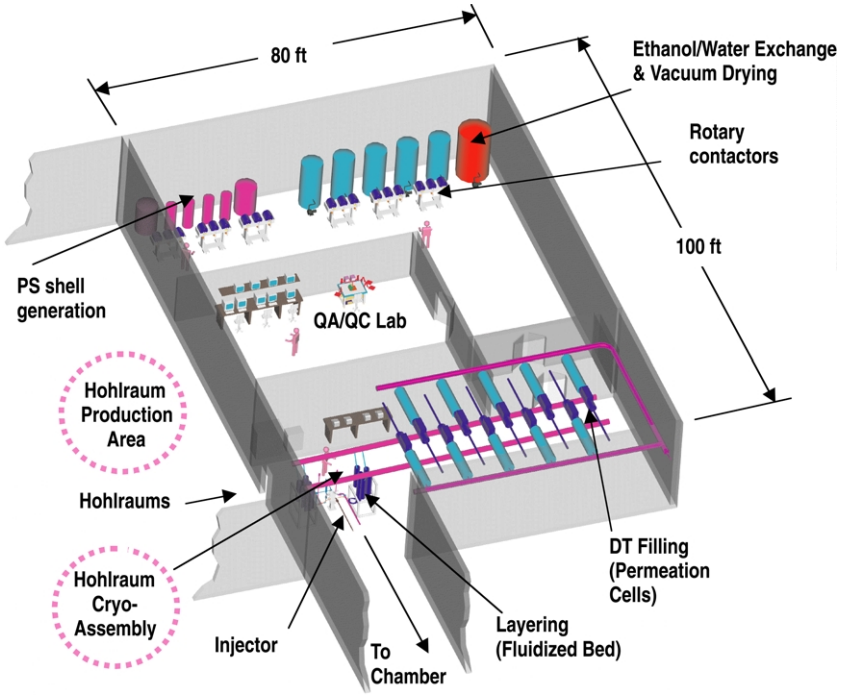

Fig. 4. Preliminary target fabrication facility layout.

The hohlraums include very low-density, high atomic number materials that are difficult to manufacture. Laser chemical vapor deposition (LCVD) is a likely manufacturing process that is being investigated by Los Alamos National Laboratory (LANL). Our study assumed that LCVD will be the primary hohlraum manufacturing process and the capital cost of LCVD equipment (estimated at $200 M) is much larger than all other equipment in the target fabrication facility combined. The total baseline estimate is $0.41 per injected target for a 1000 MW (electrical) plant, including $0.11 for filled and layered capsules. Substantially lower costs are estimated if capsules and hohlraums are fabricated for many plants off-site in a central facility.

Recycling of hohlraum materials is not recommended because the waste stream is relatively small (approximately 1 m^3/y for a 1000 MW electrical plant) and recycled materials would be radioactive and greatly increase the target fabrication costs as illustrated in Fig. 5. Figure 5 assumes that glove box handling doubles the capital cost and increases

operating costs by 50% and that hot cell processing increases capital costs by 10 times and triples the operating costs.

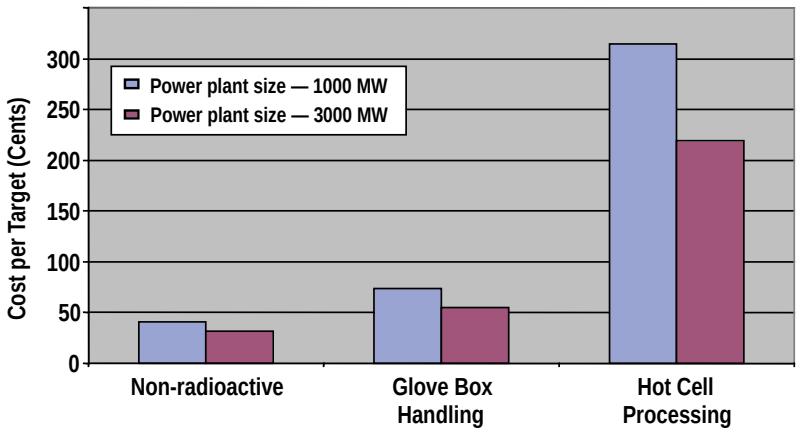

Fig. 5. Approximate cost per injected target depends on level of radiation controls required.

Approximately half of the total ($75M/Y) facility costs are from operating expenses, as illustrated in Fig. 6.

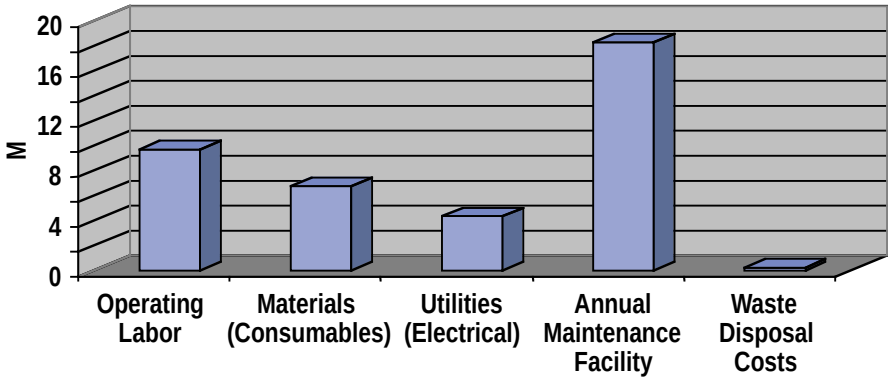

Fig. 6. Annual operating expenses for a 1000 MW electrical IFE target fabrication facility.

5.4. TARGET INJECTION

With Naval Research Laboratory funding, we completed fabrication and installation of the components required for single-shot target injection with single axis tracking. Initial single-shot testing was carried out. Most of these components, with the exception of the smooth gun barrel, can be used for both direct-drive and indirect-drive targets. We designed and ordered a unique rifled barrel for use with indirect drive target injection testing. The barrel is vented near the muzzle, has narrow lands (0.05”) and a twist of just one turn each 120”.

We performed a series of calculations pertaining to the survivability of indirect-drive targets during acceleration in a rifled gun barrel.

Cryogenic indirect-drive targets will be accelerated in a warm gun barrel. There will be of order 0.001” (0.025 mm) thermal expansion in target radius during target acceleration. It may be desirable to use a thin (0.5 mm) foam outer layer that would compress to compensate for this expansion. A foam layer would also engrave more easily in the rifled barrel than a solid material. We calculated the stress in a foam covered target undergoing angular acceleration of 126,000 rad/s^2 for various rifle land heights, widths and foam densities. As shown in Fig. 7, even in the case of 10% dense polystyrene foam with groove height and width of just 0.1 mm, the resulting maximum stress (0.15 MPa) is much less than the yield stress of the foam (0.71 MPa).

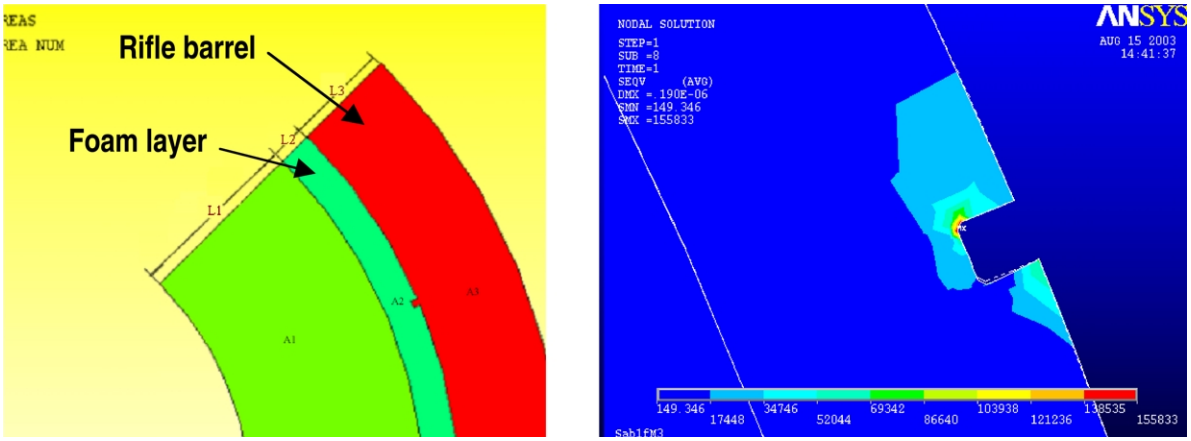

Fig. 7. ANSYS model and results for Von Mises stress in a target with a 10% dense foam outer layer undergoing angular acceleration of 126,000 rad/s^2.

To handle pressure from the gas used for accelerating an indirect-drive target, a stronger material than the very low-density foams that make up the target interior is required. This can be performed by a sabot or by a membrane attached to the pressure-facing side of the hohlraum. If a membrane is used, it should be as thin as possible to minimize the amount of driver-beam energy absorbed in the membrane. ANSYS calculations were performed to determine the resulting stress in the target and membrane for a target undergoing 10,000 m/s^2 acceleration. The minimum membrane thickness for three polymers was calculated using both cryogenic and room temperature properties as shown in Table 3.

Using a simplified model of the target, we performed preliminary calculations of the survivability of the internal foam. As shown in Fig. 8, the hohlraum was modeled with an outer polystyrene shell, a PbHf foam layer with density 0.1 g/cm^3 (E=1.26 MPa), and a PbHf foam layer with density 0.011 g/cm^3 (E=15 kPa).

TABLE 3
MINIMUM THICKNESS FOR PROPELLANT GAS MEMBRANE ASSUMING 10,000 m/s^2 TARGET ACCELERATION FOR THREE REPRESENTATIVE POLYMERS

Polymer	T = 18 K			T = 293 K		
	E (GPa)	Yield Stress (MPa)	Thickness of the Membrane (μm)	E (GPa)	Yield Stress (MPa)	Thickness of the Membrane (μm)
PS	5.41	75 (74–80)	9	1.4–3	30–35 (36–41)	15
HDPE	9.6	182 (159–179)	4	1	20–28 (31–35)	15
Nylon	9.65	200 (183–206)	3	3.5	50–110 (82–93)	6

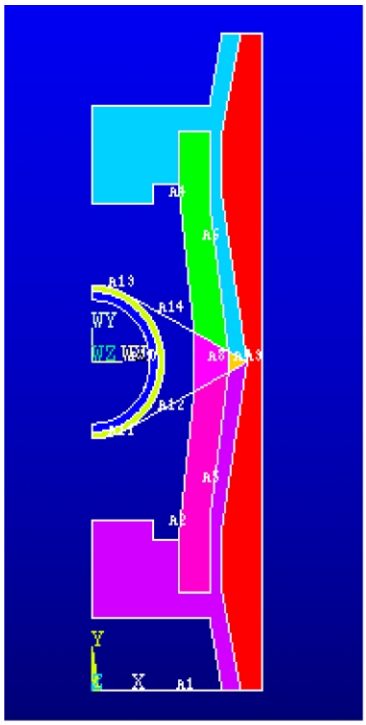

- **Density**
  - Plastic (red) – ρ = 1 g/cm^3
  - Metallic foam 1 (blue and purple) – ρ1= 0.1 g/cm^3
  - Metallic foam 2 (green and magenta) – ρ2 = 0.011 g cm^3
- **Young's modulus**
  - For calculating Young's modulus of the foams, the following procedure was used:
    ρ(Pb/Hf)=0.7 ρ(Pb)+0.3 ρ(Hf)
    ρ =12.09 g/cm^3
    E(Lead alloys)=14 10^9Pa, T=293K
    $\Rightarrow$ E(T)=E(0)*(1+a*(T/T_M,), T_M=606.6K, a = 0.5[a]
    E(18)=1.818 10^{10}Pa
- **For open cell foams:**
  E(f)=E(T)*C*(ρ_f/ρ)^2, C=0.98 [b]
  $\Rightarrow$ E(f1)=1.256 10^6 Pa, E(f2)=1.5 10^4 Pa

[a] Gibson L.J, Ashby M.F 1997. Cellular Solids: Structure and properties. Cambridge, UK.
[b] Gibson L, Mechanical Behavior of Metallic Foams. Annual Review of Materials Science. V30,2000

Fig. 8. ANSYS model for target stress and strain calculations.

To avoid collapse of the foam, the Deshpande-Fleck phenomenological criterion:

$$\sigma_{pl} \geq \delta \quad ,$$

$$\delta^2 = \left[\sigma_e^2 + \alpha^2 \sigma_m^2\right] \Big/ \left[1 + \left(\frac{\alpha}{3}\right)^2\right] \quad ,$$

is used where σ_{pl} is the plastic collapse stress, σ_m is mean stress, σ_e is Von Mises stress and α is a parameter approximately equal to two (2). The estimated collapse stress for an open-celled foam is given by:

$$\sigma_{pl} = \sigma_{ys}\ 0.3\left(\rho_f / \rho_w\right)^{3/2}$$

which for 0.011 g/cm^3 Pb is just 58 Pa. The maximum stress (δ) in the low-density foam (neglecting very small stress riser volumes) during 10,000 m/s^2 acceleration is approximately 400 Pa. This indicates a potential limit to target acceleration, but the actual strength of low-density alloys that will be used in targets may be significantly higher than our estimated values for pure Pb.

5.5. GA HOSTED MEETING

5.5.1. US/Japan Target Fabrication and Injection Workshop

We hosted the US/Japan IFE Target Fabrication and Injection Workshop February 3–4, 2003. Over 20 specialists from the United States and Japan participated in presenting recent work and program overviews. The meeting presentations and summary are available at the Web site http://aries.ucsd.edu/LIB/MEETINGS/0302-GA-IFE/.

The following invitations and activities resulted from the meeting.

1. The United States is invited to the Institute of Laser Engineering (ILE), Osaka University, for the next target workshop in October of 2004.
2. Abbas Nikroo (head of the Center for Polymer and Coatings Development at GA) was invited to and visited ILE target labs in April 2003.
   a. Abbas had a very productive two weeks at ILE starting April 14th. He was able to observe many of the target fabrication activities at ILE first hand and have very enlightening and fruitful discussions with researchers in the target fabrication group. His extended stay allowed him to closely interact with the personnel performing the hands-on work. He compiled a list for improvements of our effort in the US, based on the techniques he learned from our Japanese colleagues.
3. Japan will send Dr. Yoshida to San Diego for an extended visit to work on tracking with the injection demonstration system at GA in March 2004.
4. We will explore doing an injection demonstration with a Japanese fast ignition target on the U.S. injection tracking system.

5.5.2. Presentations at the US/Japan Workshop

Target Fabrication Session

- T. Norimatsu (ILE) — Target fabrication and injection activities toward a laser fusion reactor with wet wall
- D. Goodin (GA) — The viability of an economical target supply for IFE
- K. Nagai (ILE) — Manipulation of the microstructure of ultra-low-density TPX foams using coagulant alcohol
- Diana Schroen (Schafer) — Fabrication of divinyl benzene foam shells for laser fusion
- Chuck Gibson (Luxel) — Use of polyimide in IFE target components
- Don Czechowicz (GA) — Foam shell fabrication research at GA
- Haibo Huang (GA) — Research on fluidized beds for fabrication of IFE shells
- Brian Vermillion (GA) — Microencapsulation studies for mass production
- John Sheliak (GA/LANL) — Recent results of cryogenic DT layering studies
- Dale Hill (GA) — Fabrication of fast ignition targets
- Rich Stephens (GA) — Real world constraints on fast ignition targets
- James Maxwell (LANL) — Fabrication of HIF hohlraums by LCVD
- Jill Dahlburg (GA) — The future of fusion energy programs in the U.S.
- S. Uchida (Institute of Laser Technology, Osaka) — Use of optical phase conjugation for laser irradiation on laser fusion fuel pellets

Target Injection Session

- Sergei Krashenninikov (UCSD) — IFE chamber ionization and its effect on target heating
- René Raffray (UCSD) — Analysis of target heating during injection
- Ron Petzoldt (GA) — Status of experimental target injection and tracking system
- Ilya Agurok (Physical Optics Corp.) — Interferometric in-chamber tracking for IFE
- T. Endo (Nagoya University) — Preliminary conceptual design of a target injector for fast ignition laser fusion
- H. Yoshida (Gifu University) — Target tracking at Gifu University
- R. Tsuji (Ibaraki University) — Flying metal pipe for target transport in IFE reactor (revised)

5.5.3. IAEA Targets and Chambers Meeting Guest Editor

We performed guest editor duties for a special issue of Fusion Science and Technology, reviewing papers from the IAEA Technical Meeting on Physics and Technology of Inertial Fusion Energy Targets and Chambers (hosted at GA in June 2002). We worked with the authors and reviewers to improve the quality of the submitted papers, accepting 31 papers for publication, and forwarding accepted papers and documentation to the journal. Four of these papers were prepared at GA.

5.6. CONFERENCES/MEETINGS (NOT AT GA)

- Fifteenth Topical meeting on the Technology of Fusion Energy
  - — In Washington, D.C., November 17–22, 2002. We prepared and presented the paper "Experimental Target Injection and Tracking System".
- Third International Conference on Inertial Fusion Sciences and Applications
  - — In Monterey, CA, September 7–12, 2003. We prepared and presented the papers "Experimental Target Injection and Tracking System Construction and Single Shot Testing", "Cost-Effective Target Fabrication for Inertial Fusion Energy", and "Microencapsulation Studies for Mass Production of IFE Targets".

5.7. PUBLICATIONS/REPORTS

Petzoldt, R.W., N.B Alexander, T.J. Drake, D.T. Goodin, K. Jonestrask, R.W. Stemke, "Experimental Target Injection and Tracking System," *Fusion Science and Technology* (July 2003).

Petzoldt R.W., N.B. Alexander, T.J. Drake, D.T. Goodin, K. Jonestrask, R.W. Stemke, and B. Vermillion, Experimental Target Injection and Tracking System Construction and Single Shot Testing, Proceedings of the Inertial Fusion Science and Applications meeting, September 7–12, 2003, Monterey, CA.

Vermillion B.A., G.E. Besenbruch, L.C. Brown, D.T. Goodin, B.W. McQuillan, and M. Takagi, "Microencapsulation Studies for Mass Production of IFE Targets", Proceedings of the Inertial Fusion Science and Applications meeting, September 7–12, 2003, Monterey, CA.

Goodin D.T., A. Nobile, D.G. Schroen, J.L. Maxwell, and W.S. Rickman "Cost-Effective Target Fabrication for Inertial Fusion Energy", Proceedings of the Inertial Fusion Science and Applications meeting, September 7–12, 2003, Monterey, CA.

6. NEXT-STEP FUSION DESIGN

6.1. PHYSICS

This task provides physics analysis and other scientific and technical input to Next Step Options (NSOs) studies for the U.S. Fusion Science Program. Emphasis in this work is on options (design candidates) to obtain plasma behavior at high-energy gain and for long-duration operation pulses. The principal content of the task is to provide definition of physics and plasma operation objectives, physics and plasma science assessments and definition of physics and other design requirements for U.S. NSO studies.

Activity for this task comprises an approximately 0.1 FTE effort and has been conducted on an approximately constant level-of-effort basis. Dr. John Wesley is the principal and sole investigator at GA.

Wesley's NSO activities during FY2003 included participation in the IAEA Fusion Energy Conference in Lyon, France and in two subsequent International Tokamak Physics Activity (ITPA) meetings on MHD, plasma control and disruption. Wesley's contributions at these ITPA meetings included presentations on the use of massive gas injection for runaway-free fast plasma shutdown in ITER and reactor-scale tokamaks, in addition to plans for a new ITPA-hosted disruption database. Wesley also prepared an invited presentation on *Active MHD Control in ITER* for the 8th MHD Control Workshop, held 3–5 November 2003 at the University of Texas at Austin. Selected highlights from the presentations on these three topics follow below. Complete texts of the presentations are available from Wesley by e-mailing a request to wesley@fusion.gat.com.

6.1.1. Massive Gas Injection for Fast Plasma Shutdown

Experiments conducted during 2002 by D. Whyte *et al* in the DIII–D tokamak demonstrated the ability of massive noble gas (argon and neon) injection to provide runaway-free fast plasma shutdown under circumstances where Ar pellet injection or lesser quantities of Ar gas injection led to significant runaway production. The avoidance of runaways in the DIII–D massive-injection experiments can be understood from the fact that the total quantity of injected electrons is sufficient to satisfy the Rosenbluth 'no-avalanche' electric-field/density criterion for unconditional runaway avoidance:

$$E \leq E_c\,(V/m) = \sim 0.1 n_e\,(10^{20}\,m^{-3})$$

where E is the in-plasma electric field during disruption or fast shutdown and E_c is the electric field sufficient to balance the Coulomb drag on an electron with energy ~mc^2. As shown in Fig. 9, the electron densities achieved in the DIII–D experiments exceeded 3 x 10^{22} m^{-3} (more than 300 times the original before-injection electron density). These high densities were achieved by injecting massive amounts of Ar (~10^{-3} atm-m^{-3}) using a fast-acting valve and a 70 atm reservoir. The fact that the plasma density rise was observed to take ≤ 2 ms indicates that the 300 m/s gas jet penetrated efficiently to the plasma core and was ionized there, resulting in a prompt plasma + neutral (bound electron) density rise in ~2 ms (~0.1 thermal gas equilibration time).

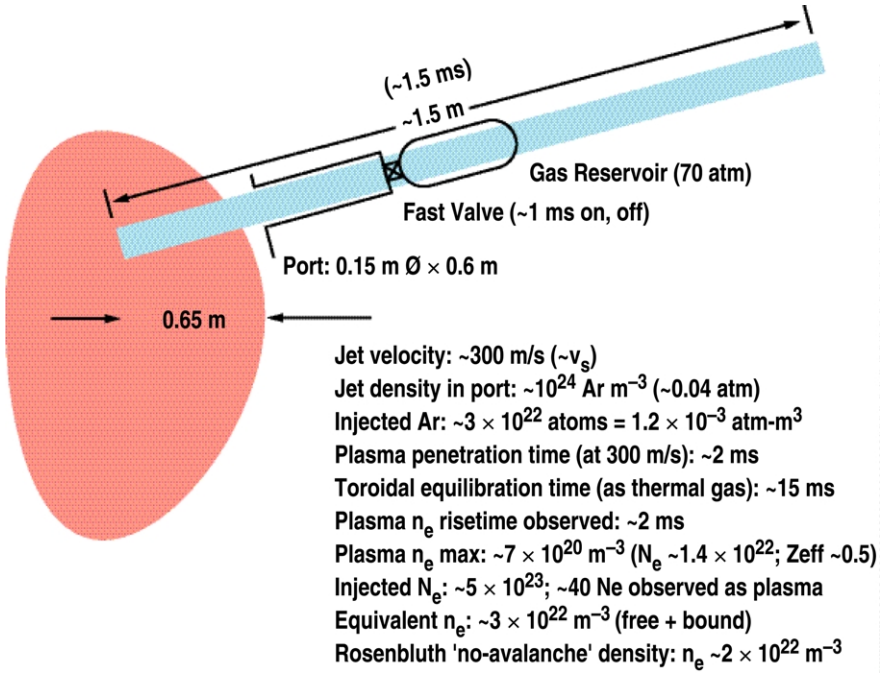

Fig. 9. Semi-schematic cross-section view and parameters of DIII–D gas injection experiment. The peak plasma densities exceed the Rosenbluth no-avalanche density and are comparable to densities predicted to yield runaway-free fast shutdown in ITER.

These DIII–D results suggest that runaway-free shutdown in ITER may be possible using similar Ar gas injection. Penetration of a 300 m/s jet into a 2-m minor radius ITER plasma will require ~5 ms, a much shorter time than the estimated shortest current quench time (~50 ms). If the DIII–D results being achieved for efficient core penetration of jet kinetic pressures $P_{jet} = 1/2\ \rho v^2 \geq P_e(0)$ scale to ITER, adequate gas penetration and densities high enough (>10^{22} m^{-3}) to satisfy the corresponding ITER no-avalanche E/n_e criterion should be achievable using foreseeable injection-valve technologies and reservoir pressures. Forthcoming (in 2004 and thereafter) plasma and jet parameter variation studies planned in DIII–D, and size and toroidal field scaling experiments planned for Alcator C–Mod and JET

during 2004, should elucidate the applicability and efficacy of massive noble gas injection for ITER runaway-free fast shutdown.

6.1.2. ITPA Disruption Database

The ITER Central Team has requested updates to the *ITER Physics Basis* [Nucl. Fusion **39**, 2137 (1999)] disruption databases (current quench rate, halo current fraction and toroidal peaking factor) and better information on thermal quench energy deposition characteristics, especially fraction of W_{th} (plasma thermal energy) to the divertor and poloidal spreading (footprint) on the divertor target. Experience during the ITER EDA showed the importance of using a 'multi-machine' database approach to setting the ITER disruption physics design basis, but also showed the limitations of simple empirical approaches: Worst-case limits were identified, but a corresponding science basis understanding could not always be obtained, and caveats were expressed about excessive conservatism. For ITER-EDA data, there was insufficient completeness and uniformity of data among the contributors to do much beyond making color-coded scatter plots (x, y plus machine ID or q_{95}, etc.). A more uniform and more comprehensive database may be able to address some aspects of the science basis lack and can also likely provide better (or more justifiable) design limits for ITER and other future conventional and low-A tokamak reactor designs. Regulatory considerations may require a more 'traceable' design-basis limit-setting approach. MHD ITPA members expect that a new disruption database (DDB) will encourage model development and validation over a wide range of machine sizes, operation regimes and aspect ratios.

Wesley's task activities in the 3rd quarter of FY2003 focused on developing plans for an International Tokamak Physics Activity DDB, to be hosted at ITPA request, by GA Fusion on behalf of the ITPA Topical Group on MHD, Disruption and Control. During the 3rd Quarter, Wesley worked with GA Fusion and DIII–D National Fusion Program staff to quantify data archiving and retrieval needs for the DDB. GA Fusion and DIII–D National Fusion Program management subsequently agreed to make the required computer and data acquisition staff-resources available to support starting the DDB in September 2003.

Wesley prepared a presentation on the DDB concept and plans for the 5th Meeting of the MHD, Disruption and Control Group held in St Petersburg, Russia, on 15–17 July 2003. The plan is to develop a comprehensive relational database that links data on disruption precursor, thermal and current quench, and runaway electron conversion with machine and parent plasma state characteristics and with ensuing disruption effects data. Wesley hopes that both conventional and low-aspect-ratio tokamaks (*aka* spherical tori or STs) will contribute. Contributing ITPA devices and institutions have made a commitment to contribute data and have identified a data contact person for each device and/or contributing institution. There was also a lively discussion of the pros and cons of soliciting general versus more focused topical data sets, and recognition on the parts of the ITPA meeting participants that the key to a successful database will be providing the contributing devices and institutions with 'data

mining' tools to facilitate efficient extraction of data from individual device databases and verifiable (by the contributors) 'quality-checking' of the extracted data.

6.1.3. Active MHD Control for ITER

ITER is now seen as "the way" to advance magnetic fusion science and technology to the burning plasma regime. The mission objectives for ITER encompass the achievement of high-gain fusion burn ($Q \geq 5$; $Q = 10–\infty$ is expected/desired) and the extension of well-controlled burn to "steady state". "Steady state" denotes full non-inductive current sustainment, with all plasma conditions stationary, maintained with reactor-compatible control means. Active control of up to four classes of MHD instability — internal $m = 1$, $n = 1$ 'sawtooth' relaxation oscillations, neoclassical tearing modes (NTMs), edge-localized relaxation modes (ELMs) and resistive wall modes (RWMs) will be required to achieve ITER objectives. Active MHD control will be mandatory for both high-Q ELMing 'baseline' H–mode and hybrid scenarios and for high-beta AT steady-state scenarios.

The need for active MHD control is recognized by the ITER design team, and the present (2001 FDR) design incorporates provisions that can, in principle, provide the control required. In terms of the four classes of instability, the provision of up to 20 MW of rf current-drive power in both the ion-cyclotron and electron-cyclotron frequency regimes should be capable of addressing the sawtooth and NTM control needs (sawtooth can be controlled by ICCD or ECCD, NTM by ECCD). However, present estimates concerning the levels of ECCD power required for NTM control suggest that 20 MW of installed power may be marginal (or sub marginal) for robust NTM control, particularly if both the 3,2 and 2,1 modes must be controlled simultaneously, as may be required for the ITER 'EMLy H–mode' baseline scenario. Simultaneous control would also require splitting the EC power into two independently steerable launcher beams (directed to two separate radial positions within the ITER plasma). These provisions are not yet incorporated into the ITER EC system design.

There are also open physics-basis questions about the ability of ICCD to address ITER needs for sawtooth control. While ECCD targeted at the $q = 1$ radius is known to be effective for sawtooth control, it is again not clear whether the ITER EC system is capable (both in terms of total power and independently steerable launchers) of providing simultaneous sawtooth and NTM control.

ELM control (reduction in energy magnitude and/or total suppression of Type I ELMs) by active means has so far been demonstrated in present tokamaks by periodic vertical position perturbations (in TCV and ASDEX-U) and by injection of multiple low-velocity pellets into the plasma edge (in ASDEX-U). Recent (2003) experiments in DIII–D have also demonstrated the possibility of nearly complete suppression of ELMs by the application of ergodic magnetic fields in a radially localized region near the plasma edge. Each of these ELM control techniques has its pros and cons with regard to efficacy and application to

ITER. The ergodic-edge method will likely require provision of specialized ‘modular’ coils located close to the plasma surface, likely inside the ITER torus vacuum vessel. Adding such coils is conceptually possible but will have a substantial impact on the present ITER design.

RWM control will be needed to allow ITER to operate in a steady-state-capable high-bootstrap-current-fraction AT (Advanced Tokamak) mode. Present successes in RWM control in existing tokamaks are largely attributable to suppression of RWMs by relatively high rates of plasma rotation. However ITER plasma rotation rates are predicted to be lower, and hence rotational stabilization may not be sufficiently effective. The present ITER design incorporates a set of external (outside the torus vacuum vessel) non-axisymmetric ‘error field’ control coils that may also be sufficiently effective to allow direct (magnetic feedback) stabilization of RWMs in the ITER AT regime. There are, however, concerns that these coils may not be sufficiently well coupled to the plasma to provide reliable RWM control. These concerns are especially high in situations where ‘plasma noise’ present in the RWM sensors and/or bandwidth limitations in the active power supplies used to drive the external coils may limit the usable system gain and hence the prospects for reliable RWM control.

RWM coils internal to the ITER vacuum vessel are predicted to offer a better RWM control margin and much lower system power levels to achieve a given control margin. However, the validation in present experiments of the physics and engineering (power supply response) models that are necessary to evaluate ITER RWM feedback control is still a matter of ongoing R&D, so drawing conclusions about the adequacy of the present external coil system is premature. It is clear, however, that adding an internal coil system will provide an additional degree of control margin and control flexibility that will, at very least, be a useful tool for ITER ‘AT/SS’ experimental studies. But again, adding such a coil system will have significant design impact.

In summary, active control of up to four classes of MHD instability will be required to achieve ITER objectives. Active MHD control will be mandatory for both high-Q ‘baseline’ and long-pulse AT/SS scenarios. The present design of ITER incorporates provisions for the various rf-current-drive and magnetic control ‘actuators’ needed for active MHD control in each of three possible operation regimes (scenarios). ECCD and ICCD are available for active MHD control. There are concerns about the adequacy and flexibility of the ECCD capabilities. More EC power and/or launcher position(s) and launch angle flexibility may be needed. These changes will have modest design impact(s).

How to best achieve active control of ELMs remains an open physics R&D issue. A need for modular in-vessel coils will have significant in-vessel design impacts. Reliability of in-vessel coils has been a long-standing point of contention within the ITER central team.

Robust RWM control is critical for ITER AT/SS success. The present ex-vessel coil system may or may not be adequate for feedback-only control, and the supplemental benefit

of rotation is uncertain. These are major RWM community/ITER team issues that require R&D in present tokamaks and in modeling for prompt resolution.

6.2. ENGINEERING

This task provides engineering management and technical input for the Fusion Ignition Research Experiment (FIRE) and other Next Step Option (NSO) systems, for example, the International Thermonuclear Experimental Reactor (ITER). One of the main activities in FY03 was the review of the ITER magnet design documents and preparation of a cost estimate for the ITER central solenoid (CS). During FY03, the effort by R.J. Thome of GA as engineering manager for FIRE decreased steadily in anticipation of FY04 funding constraints.

The magnet systems for the ITER long-pulse tokamak are among the largest and most expensive components. They comprise the toroidal field (TF) and poloidal field (PF) coils, the CS, and the correction coils. Together they confine, shape and control the elongated, poloidally diverted plasma capable of producing 500 MW of DT fusion power for 400 s. Superconducting coils representative of future steady-state reactors are used to keep electrical power consumption acceptable for ITER. The ITER magnets were designed between 1993 and 2000, with major U.S. participation until 1998. The most critical coils are the TF coils and the CS, due to their size, high magnetic field, and cost.

The CS produces most of the 277 V-s flux change that generates and maintains the 15 MA plasma current in the inductive mode, as described in the ITER Plant Description Document. In so doing, the CS sees a complete inversion of field from +13.5 T to –12.8 T at mid-height. The currents distributed in the six independent modules of the CS also help shape and stabilize the plasma.

The configuration of the ITER CS assembly, located at the core of the tokamak and supported by the toroidal field coils, is shown in Figs. 10 and 11. The CS assembly consists of a vertical stack of six winding packs (modules). It is centered and hung from the top of the toroidal field coils through radially flexible supports. It is braced to the bottom of the TF coils against dynamic horizontal forces. The six modules are placed in compression by a vertical preload structure.

The ITER CS will be a large-scale, state-of-the-art, high-field, pulsed (13 T), superconducting magnet system. The six 110 t modules could be supplied by the United States to contribute to both the world fusion program and to superconducting magnet technology development in U.S. industry. The CS will use an advanced niobium-tin (Nb_3Sn) superconductor, a high nickel steel jacket for the conductor, and complex fabrication techniques requiring advanced tooling and procedures. The features of the CS are summarized in Table 4.

The United States supplied a close-to-full-scale 13 T module as part of the ITER EDA. This CS Model Coil has been successfully operated in a pulsed mode in a facility in Japan as part of a three-year test program and is a major accomplishment in superconducting magnet development.

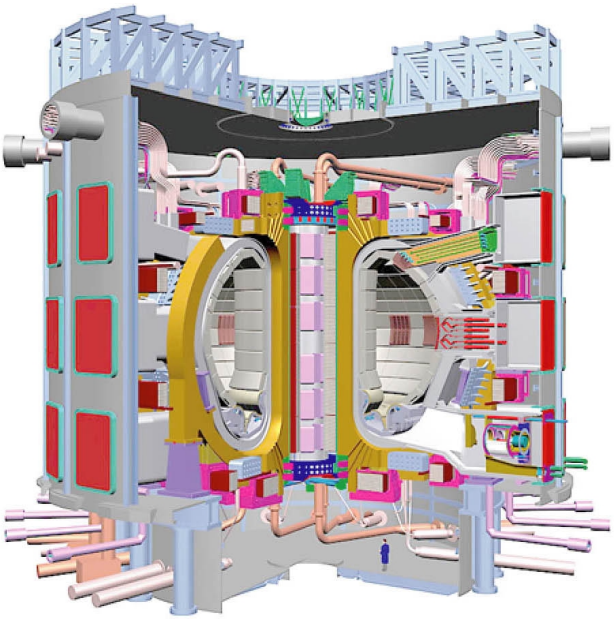

Fig. 10. The 12.6 m-high, 660 t, 13 Tesla Central Solenoid located in the central bore of the ITER Tokamak is visible in this cutaway view.

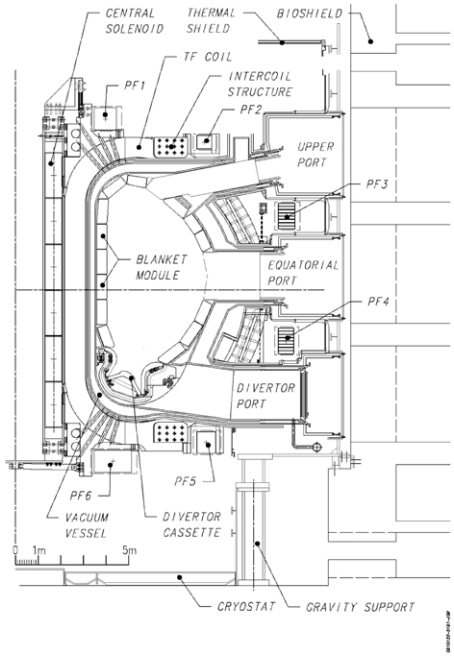

Fig. 11. This cross-section shows the six 110 t-modules of the Central Solenoid, stacked at the center of the ITER tokamak.

TABLE 4
FEATURES OF THE ITER CENTRAL SOLENOID

Central Solenoid	Winding configuration	6 modules
	Overall coil height (excluding structures)	12.1 m
	Overall coil outer diameter	4.15 m
	Overall weight (including structures)	840 t
Module (1 of 6)	Inner diameter	2.6 m
	Outer diameter	4.15 m
	Height	2 m
	Module Weight	110 t
	Conductor unit length	812m
	Total conductor length	5682m

Like the TF coil conductor, the CS conductor contains a multistage circular cable with about 1000 strands of Nb_3Sn (to operate at high field) and pure copper strands (for quench protection). The stages are cabled around a small central spiral cooling tube, and the cable is contained in a thick structural conduit with a square outer cross-section. The conductor, cooled at 4.5 Kelvin by a flow of 0.6 MPa supercritical helium, carries a peak current of 46 kA. Unit lengths of conductor are wound one-in-hand into superposed multiple pancakes connected in series to form each of the six modules. The total conductor length used to wind the six CS modules is about 34,000 m. The CS conductor is almost identical to the conductor already used for the CS model coil, but will have a more advanced Nb_3Sn wire due to developments in the industry since the model coil wire was specified in 1993.

With its turn-, pancake-, and ground-insulation composed of polyimide film, fiberglass tape, vacuum-pressure-impregnated resin and conductor, a completed module weighs approximately 110 tons. The insulation can withstand at least 5 kV to ground in normal condition and 10 kV to ground in fault condition. The internal electrical joints between multiple pancakes are located at the CS outer diameter and at the helium inlets at its inner diameter. The terminal electrical joints and helium outlets of the six modules are located at the top and bottom of the CS.

Each CS module is connected to its own power supply and protection system, the cryoplant, and the data acquisition system via an in-cryostat CS feeder, a cryostat feedthrough, and a coil terminal box located outside the cryostat. Similarly, in-cryostat feeders and cryostat feedthroughs connect the CS structures to structure cooling valve boxes located outside the cryostat.

The CS instrumentation and control system:

- Measures the cooling and thermo-hydraulic parameters, and calculates the required coolant mass flow rates,
- Monitors the CS operating parameters and notifies the operator through the alarm system if set points are exceeded,
- Detects superconductor quenches, electrical faults, and other abnormal conditions, and triggers protective energy discharges through the plant interlock system.

During FY03, F. Kimball, J. Wohlwend, D. Paganini, and R.J. Thome reviewed the ITER design documentation and produced a report outlining manufacturing processes and a schedule for the CS. Results were provided in a report, "ITER Central Solenoid Coil Manufacturing Cost and Schedule Estimate", GA–C24384 July, 2003.

6.3. THERMAL FATIGUE ANALYSIS OF FIRE DIVERTOR SEGMENT

Thermal stress analysis of the FIRE divertor prior to 2003 was based on a calculated peak heat flux of 25 MW/m^2 on the outer divertor. This analysis is summarized in Ref. 4.

Better understanding of the operating scenario resulted in new heat flux profiles calculated by M. Ulrickson [5] and are shown in Fig. 12. The new values of power flows are listed in Table 5. The geometry of the divertor and baffle is summarized in Table 6.

Due to reduction in peak heat flux values, the flow velocities required to avoid the critical heat flux (CHF) have been reduced. Therefore the total flow required has also gone down from 288 l/s to 173 l/s. The new results are shown in Table 7.

Data:

- Water Inlet Temperature = 30°C
- Pressure = 1.5 MPa
- Number of Modules = 32

TABLE 5
POWER FLOWS

	Outer Divertor	Baffle
Total power (MW)	34.3	10.7
Peak power/module (MW)	2.32	0.58
Peak heat flux (MW/m^2)	7.5	3.5
Nuclear heating in W (W/cm^3)	42	34
Nuclear heating in Cu (W/cm^3)	16	13

TABLE 6
GEOMETRY

	Outer Divertor	Baffle
Number of modules	32	32
Number of coolant channels per module	48	30
Coolant channel diameter (mm)	8	10
Cooling cell width (mm)	14	21
Heat transfer enhancement	Swirl Tape, thickness = 1.5 mm, twist ratio = 2	None

TABLE 7
RESULTS OF THERMAL HYDRAULIC ANALYSIS

	Outer Divertor	Baffle
Number of coolant channels in series	2	2
Maximum PFC temperature (°C)	TBD	TBD
Maximum copper temperature (°C)	TBD	TBD
Flow velocity (m/s)	6	3
Flow/module (l/s)	5.4	3.5
Exit coolant temperature (°C)	138.3	127
Exit pressure (MPa)	1.34	1.48
Exit sub-cooling (°C)	54	120
CHF (MW/m^2)	27	13.6
Maximum wall heat flux (MW/m^2)	TBD	TBD
Safety factor on CHF (estimate)	> 2	> 2

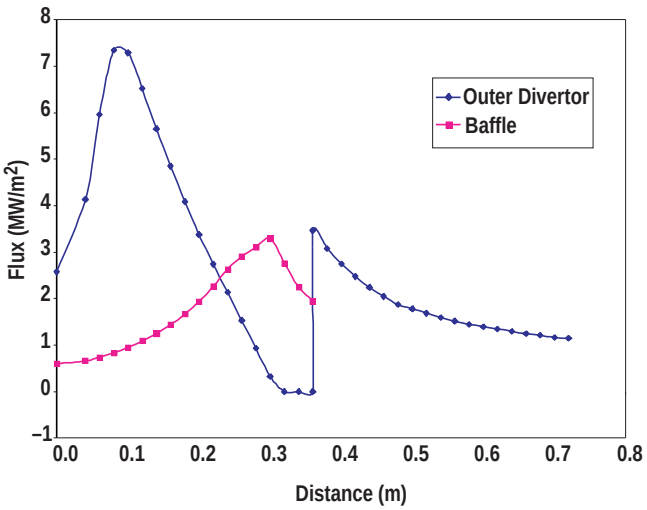

Fig. 12. Heat flux distribution on FIRE divertor and baffle.

7. ADVANCED LIQUID PLASMA SURFACE (ALPS)

GA continued to support the ALPS program, managed by Argonne National Laboratory (ANL), by coordinating the task of Tokamak Experiments and Lithium-Divertor Materials Evaluation System (Li-DiMES) experiments. We provided atomic data support to the ALPS edge-physics modeling group. We also provided further analysis to the innovative liquid and solid-surface fusion power reactor divertor designs.

7.1. HIGHLIGHTS

- Preliminary 2-D modeling results indicate that, with a good conducting path, the undesired injection of lithium (Li) into the plasma core could be reduced.
- We completed the design and fabrication of the Li-DiMES sample. The experiment was proposed to DIII–D.
- Four specialized computer codes have been coupled successfully to model Li sputtering and transport from a DIII–D DiMES sample.

7.2. Li-DiMES SAMPLE DESIGN

The DiMES team was on a fast track to develop a Li-DiMES sample for the proposed heated and wetted Li experiment. Our technical goal was to understand the magnetohydrodynamic (MHD) interaction between the parallel current and the liquid Li at the lower divertor of DIII–D. Scientists from Sandia National Laboratories (SNL)–Livermore, GA and SNL–Albuquerque had proposed different designs for the sample. The selected approach consisted of an electrically isolated boron nitride (BN) holder with Li material held in two separate, electrically floating and grounded slots in order to see the difference between the two cases. We will try to repeat the disruption-induced experiment with liquid Li and provide a radial array of scrape-off-layer (SOL) current-monitors for current-profile measurements.

UCSD performed Li-wetting tests with different materials. Different options for sample temperature control were assessed. Resistance of the connecting wires inside the DiMES mechanism were carefully measured and documented, leading to the recommended use and subsequent modification of a higher resistance heater for the Li-DiMES module in order to decrease power deposition in the connecting wires. Upon presentation of the initial design, the DIII–D experiment review committee posed minor questions about certain aspects of the design. These questions were addressed by subsequent design modifications that were communicated to and ultimately approved by the committee.

Following committee approval, SNL completed the fabrication of the Li-DiMES sample, shown in Fig. 13. Graphite and B_4C parts were out-gassed at GA. The metallic connectors design was modified at SNL-Livermore to make the connectors more flexible in order to accommodate the dimension change during sample insertion. The sample will be tested at GA before insertion into DIII–D, and the first sample will be inserted without Li for the testing of temperature control and the measurement of title currents.

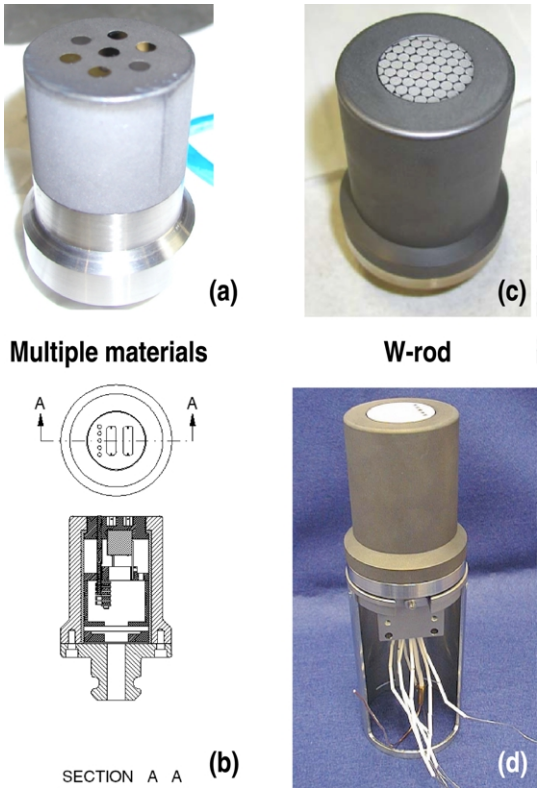

Fig. 13. DiMES samples.

7.3. Li-DiMES

7.3.1. Exposure Analysis

Li-DiMES camera data was resurrected and analyzed for DIII–D shots 105506 through 105511. It was found that the solid Li sample melted during the first shot (105506) with a swept strike point. The sample had clearly melted, flowing across most of the DiMES probe head and onto an adjoining tile. The plasma did not disrupt on this shot and there was relatively little evidence of the Li injection on any of the baseline diagnostic systems. In continuing analysis of the shots, equilibrium fitting (EFIT) data was used to calculate the position of the outer strike point relative to the Li sample as a function of time. A detailed analysis of Li I (λ=671 nm) spectroscopic data from shot 105508 was completed. The data is

consistent with a distributed Li source caused by melting due to the outer strike point swept across the DiMES sample. A large emission spike saturated the spectrometer at t=3937 ms. The spike appears to be the signature of a small, liquid-Li droplet that is ejected when the strike point is directly over the Li sample. The direction of the Li movement in the DiMES video data is consistent with the creation of a radial current path capable of producing the JxB force necessary to eject a small droplet into the divertor plasma. This force was apparently smaller than the one seen during the disruption of shot 105511.

7.4. MHD MODELING SUB-GROUP

Preliminary 3-D MHD modeling results reported by UCLA showed encouraging results for a period of 1.5 ms. Results show that the MHD effect can cause radial movement of the Li in the rectangular container, spilling over on one end and emptying the Li out the other. These results correspond to the geometry of the new experiment. The run time for this calculation will be extended to include the effects from plasma heating.

7.5. MODELING AND ANALYSIS

Four specialized codes were coupled successfully to model Li sputtering and transport from a DIII–D DiMES sample. Background plasmas were simulated with the B2.5 /DEGAS fluid plasma, which is a kinetic neutral deuterium, and the code was run by L. Owen and R. Maingi of Oak Ridge National Laboratory (ORNL). Li sputtering sources were simulated with the gyro-kinetic WBC code run by J. Brooks of ANL and coupling the kinetic Monte Carlo Impurity (MCI) code, run by T. Evans of GA, and D. Finkenthal of Palomar College, simulated Li transport. Preliminary Li transport results indicate a core concentration increase ranging from 0.0002% to 0.1%, depending on T_e in the private flux region. While this variation is large and the results are very sensitive to the boundary conditions used in the fluid code, the results are in agreement with experimental data indicating that there is always less than 1% Li in the edge plasma during the discharge being simulated.

An analysis of the neutral Li mean-free-path variation in DIII–D shot 105508 was performed using a b2.5 /Degas plasma solution and new Li ionization data from the Atomic Data and Analysis Structure (ADAS). We found that neutral Li sputtered from various parts of the solid Li-DiMES sample during the strike point sweep in shot 105508 had penetration depths ranging from about 0.4 cm to 5.7 cm, while the D^+ flux hitting the Li sample ranges from $3.7*10^{22}$ m^{-2} s^{-1} at the outer edge to $8.5*10^{20}$ m^{-2} s^{-1} at the inner edge. These two effects tend to cancel each other during the sweep, but this analysis highlights the fact that the strike point sweep makes the modeling much more complex and difficult to interpret. We therefore recommend not using strike point sweeping during experiments in which data is being acquired to benchmark numerical modeling.

7.6. ATOMIC DATA AND ANALYSIS STRUCTURE (ADAS)

ADAS Li-II emissivity data was supplied to D. Whyte of the University of Wisconsin for a Li-DiMES transport analysis. We also assessed the accuracy of this data since it appears to be in disagreement with the experimental observations, assuming the sputtering source and Li I spectroscopic analysis are correct.

Work continued on modeling Li 2p-2s emission (λ=671 nm) measured during shot 105508. We are working with the Atomic Physics Group at Auburn University on a detailed ionization balance calculation to be compared with the DIII–D MDS data.

T. Evans had discussions with D. Schultz of ORNL about Li atomic data modeling at the International Plasmas Edge Theory Workshop on September 3rd. Schultz was asked to look at ways to calculate the emission coefficient for high n neutral transitions of Li.

7.7. PFC PROGRAM PLANNING

As a member of the steering committee (SC) of the US-PFC program, C. Wong worked on the evaluation of proposed US-PFC tasks and budget for 2004. The first agreement from the SC was reached and the recommendations were sent to DOE. Sam Berk of DOE then asked us to perform a bottom-up and prioritized assessment in the next iteration.

8. ADVANCED POWER EXTRACTION STUDY (APEX)

In FY2003 we completed the recirculating FW/blanket design and participated in the planning of the U.S. participation in the ITER test module program. We reviewed proposed-designs from the European Union, Japan and Russian, and helped to formulate our U.S. proposals.

8.1. HIGHLIGHTS

- We completed the overview paper for the Advanced Power Extraction (APEX) task IV recirculating FW/blanket design and prepared a section for Dr. Mohammed Abdou's overview paper. Both of these papers have been submitted to the Journal of Fusion Engineering & Design.
- A helium closed-cycle system with four compressors and two turbines was selected as the reference power conversion option for the recirculating FW/blanket design. This system can lead to a gross thermal efficiency of 46.9%.
- With the inclusion of MHD effects, the AFS/FLiBe first wall blanket module has a system pressure of 1.4 MPa. Corresponding stress analysis results indicate that our reference design can meet both primary and secondary stress limits.

8.2. RECIRCULATING BLANKET DESIGN

As a research element for the APEX program, the solid first wall and blanket design team assessed innovative design configurations with the use of advanced nano-composite ferritic steel (AFS) as the structural material and FLiBe as the tritium breeder and coolant. The goal for the assessment is to search for designs that can have high volumetric power density and surface heat-flux handling capability, with assurance of fuel self-sufficiency, high thermal efficiency and passive safety for a tokamak power reactor. We selected the recirculating flow configuration as our reference design. Based on the material properties of AFS we found that the reference design can handle a maximum surface heat flux of 1 MW/m^2, and a maximum neutron wall loading of 5.4 MW/m^2, with a gross thermal efficiency of 47%, while meeting all the tritium breeding, structural design and passive safety requirements. Our work covers the results of the following areas of assessment: material design properties; FW/blanket design configuration; materials compatibility; components fabrication; neutronics analysis; thermal hydraulics analysis including MHD effects; structural analysis; molten salt and helium closed-cycle power conversion system; and safety and waste disposal of the

recirculating coolant first wall and blanket design. Critical issues remain in the areas of the compatibility temperature between Pb and AFS and structural design of the poloidal module.

8.3. MATERIALS COMPATIBILITY

To increase the interface allowable temperature between AFS and the Pb neutron multiplier, we proposed to protect the AFS surface with a thin coating of tungsten, which could then allow us to operate the temperature at > 700°C.

8.4. FABRICATION

A fabrication method of high-pressure diffusion bonding was reviewed for the oxide dispersion AFS FW/blanket modules, and found to be applicable. Two fabrication procedures were proposed for the design.

8.5. STRESS ANALYSES

M. Friend of GA compared the difference between circular and the reference square front first wall channel designs. The pressure in the large central ducts leads to slightly larger stresses in case of the circular channel, but still manageable. For neutronics reasons, we selected the four front channels design (the Pb-fraction will probably be too small with five channels). With a coolant outlet temperature of 683ºC and coupled to a Molten Coolant Gas Cycle multiple reheat and cooling power conversion system, a gross thermal efficiency of 47% can be projected.

8.6. HEAT TRANSFER

M. Mogaheds of the University of Wisconsin analyzed the alternative FW design with circular concentric tubes with the Pb-multiplier tube located in an eccentric arrangement. After a number of iterations, he showed that the maximum tube temperatures, the maximum interface temperatures, and the temperature variations around the tube could be reduced by this configuration without increasing the pressure drop.

8.7. MHD CALCULATION

With the inclusion of MHD effects, the first wall and blanket fluid pressure drop was increased and the total system pressure was increased to 1.4 MPa. Stress analysis of the design indicates that our reference design can meet the primary and secondary design limits for the AFS materials.

8.8. MOLTEN SALT COOLED GAS CYCLE (MCGC)

J. Bolin of GA evaluated the MCGC by looking at the options for different combined use of compressors and turbines. A four compressors and two turbines system which can lead to a gross thermal efficiency of 46.9% was selected as the reference option.

8.9. TRITIUM CONTROL

After a number of design iterations with INEEL engineers we resolved all the serious tritium control problems for the recirculating FW/blanket design. These modifications include: (a) Reduction, by orders of magnitude, of tritium implantation into the first wall by taking the sticking coefficient for sputtered steel or tungsten coating instead of slightly oxidized steel. (b) Use of triple concentric tubes for coolant access pipes, resulting in low temperature outer tube, low partial tritium-pressure in the outer He-channel, and low heat losses from the hot outlet to the cold inlet FLiBe flow. As a result, tritium-losses into the containment atmosphere are of no problem during both normal operation and during accidents. Furthermore, the He-mantle around the coolant access tubes and all external components of the cooling loops can serve as guard heating for preheating and to keep the FLiBe liquid under design conditions. (c) Use of Al-tubes in the heat sink where the tube temperature is <70ºC results in negligible low tritium permeation rates.

8.10. ITER TEST MODULE PROGRAM

S. Malang reviewed the ITER test module concepts proposed by EU, Japan and Russia. There are a total of six concepts. He included the new concepts being worked on in the United States, with a total of 10 concepts. Wong also asked him to review in depth two critical issues: the selection and development of solid breeder and the development of LiPb as the breeding material. The report was prepared and the information had helped us to go on a fast track evaluation and selection of U.S. reference and back-up blanket concepts for our ITER test module program.

8.11. PAPER PREPARATION

We completed the GA review of the recirculating flow FW/blanket design overview paper. It was sent to Mohamed Abdou to be submitted to the Journal of Fusion Engineering and Design for review.

We also completed the first draft of a section for the APEX program review paper to be put together by M. Abdou.

8.12. MEETING

The U.S. high power density workshop was hosted by C. Wong at UCLA. There were about 20 participants from Japan and the United States.

9. PLASMA-FACING COMPONENTS — DiMES

The Divertor Materials Evaluation System (DiMES) program at GA has been using a sample changer mechanism to expose different ITER-relevant materials to the lower divertor of DIII–D to study integrated plasma materials interaction effects in a tokamak and to benchmark modeling codes. Over the years we found that for carbon, detached plasma would reduce the maximum erosion rate but its redeposition could still be too much for ITER because of the corresponding tritium inventory. Interestingly, even with the reduction of carbon erosion from the divertor, the core carbon concentration remains about the same. The additional carbon source from DIII–D could be from the first wall. From the study of chemical sputtering, we learned about the potential impacts from the aging of the first wall material. When Li was exposed at the divertor we found significant and complicated MHD interactions between the parallel current in a tokamak and the conducting liquid. This report presents our continuing activities in 2003 in response to the needs for the plasma facing components (PFC) design for advanced tokamak machines like ITER.

9.1. HIGHLIGHTS FOR 2003

- With support from DIII–D, we completed the repair and recovery of the DiMES sample changer system. Damaged programmable logic controller (PLC) module and vacuum controllers were replaced; and the sample changer system was restored to a robust operational state.
- Dr. Dmitry Rudakov of UCSD has joined the DiMES team as the DiMES experimental coordinator.
- We successfully exposed a Si-doped depth marked graphite sample to a DIII–D disruption. This is to simulate the impacts from ITER-ELMs on the graphite surface. Measurable erosion was reported by SNL.
- A multiple-materials DiMES sample was exposed to 22 upper single null discharges to simulate effects from chamber wall erosion.
- The DiMES hydrogen sensor and the W-rod samples passed the physics and engineering review by the DIII–D review committee.
- An experiment on sampling the coating from DIII–D boronization was performed successfully.

9.2. DiMES SYSTEM MAINTENANCE

A new fixture to hold the DiMES system bellows in place was delivered in December of 2002. It was checked and installed. Subsequently, the DiMES sample changer mechanism was disassembled and the outer coating of the internal cable was found to be severely corroded, causing the hydraulics system to malfunction. The cable was replaced and the system was cleaned, reinstalled and aligned. The primary vacuum valve was also replaced. The DiMES system was returned to fully functional form. The first experiment on sampling the coating from DIII–D boronization was performed successfully.

9.3. DiMES INSTRUMENTATION

The DiMES electrically isolated instrumentation rack was installed at the lower pit of DIII–D. The rack houses a heater power supply and related electronics. In the future it could also accommodate a dedicated data acquisition system.

9.4. EXPERIMENTS

9.4.1. Disruption Experiment/ITER ELMs Simulation

A depth-marked graphite sample was exposed to a single vertical displacement event (VDE) disruption. The heat flux at the radius of the sample was measured by an IRTV operating in a fast scan mode. Ion flux at the radius of the probe was measured using a Langmuir probe. The heat and particle fluxes during a DIII–D disruption are similar to those expected in a type-I ELM on ITER. Erosion of the graphite surface was determined by Sandia National Laboratory (SNL) by measuring the shift in the depth of an Si marker measured by Rutherford Back Scattering (RBS) with a two MeV He^4 ion beam. Measurements were made along scans in the radial and toroidal directions through the center of the probe in 2 mm steps. Results are shown in Figs. 14 and 15. Results show that the erosion was very small, which is good news for ITER. The average and standard deviation of the values shown in the plots is 7 ± 4 nm. Usually, $\pm$ 10 nm would be the detection limit, which corresponds to about a 3% shift in the Si marker depth.

9.5. MULTIPLE MATERIALS EXPERIMENT

A multi-material probe, as shown in Fig. 13, was exposed to the scrape off layer (SOL) plasma during upper single null operation in L–mode. This probe contains mini-samples with W, Be, and V coatings, as well as bare graphite samples. The probe was exposed to 22 discharges, as the erosion rate from SOL exposure is expected to be small. The goal is to measure the erosion (or redeposition) from the plasma facing wall in the main chamber. The exposed sample was sent to SNL for erosion measurement.

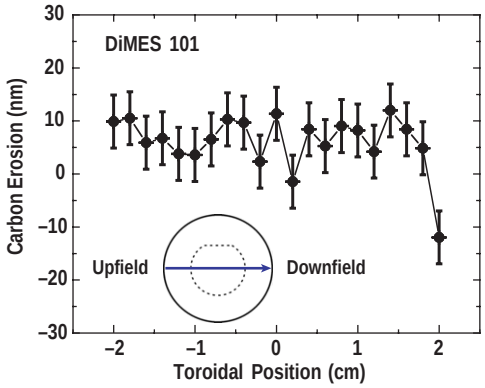

Fig. 14. Carbon erosion in the toroidal direction.

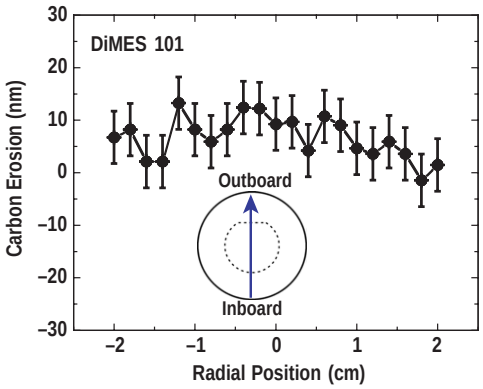

Fig. 15. Carbon erosion in the radial direction.

9.6. HELIUM DISCHARGES

A depth marked DiMES sample was exposed to a series of lower single null (LSN) discharges in He with as-simple-as-possible plasma discharges to study carbon erosion by the He plasmas. Results of this experiment will be compared with deuterium discharges. The exposed sample was also sent to SNL.

9.7. BORONIZATION EXPOSURE

A DiMES sample was successfully exposed to DIII–D boronization and the boronized coating has been analyzed.

9.8. DIAGNOSTICS DEVELOPMENT SUPPORT

A DiMES sample with a built-in flush mount (flat) Langmuir probe was used in a piggyback experiment to compare the performance of a flat probe to that of dome-shaped ones.

9.9. SAMPLE PREPARATION

9.9.1. Hydrogen Sensor

Bob Bastasz and Josh Whaley of SNL/Livermore gave an excellent physics and engineering review of the DiMES sample design of the hydrogen-sensor experiment to the DIII–D review committee. This experiment measures the hydrogen neutral particle flux to the first wall and the divertor. We are finishing the preparation of this sample and the corresponding supporting instrumentations before insertion into DIII–D.

9.9.2. W-rod Experiment

Supported by an estimate on the erosion rates of the W-metal under different DIII–D operating conditions, we passed a vacuum and physics committee review on the exposure of the W-rod sample from SNL. A picture of the sample is shown in Fig. 13. We will be allowed to expose the sample to as many as 50 discharges, but during the experiment we will have to carefully monitor the potential W-emission from the core.

9.9.3. Be Exposure Hazardous Work Authorization

In response to the request of the DIII–D safety committee, we considered and adopted the use of a thinner Be coating of 20 nm in order to reduce the amount of possible eroded Be that could be redeposited in the DIII–D chamber. This satisfies the more stringent allowable volumetric Be concentration regulation from DOE and OSHA.

9.10. MEETINGS

C. Wong attended the High Heat Flux Components and Plasma Surface Interactions in Next Fusion Devices U.S./Japan exchange workshop, Nagoya, Japan, December 7–13. He made three presentations: (1) on the Boundary Physics of DIII–D, a year-end review; (2) DiMES program status and planning; and (3) an idea: A multi-materials approach on the tokamak FW/divertor surface design.

9.11. DiMES PROGRAM PAPER

A paper on “Experimental observations of lithium as a plasma-facing surface in the DIII–D tokamak divertor” by D.G. Whyte, T.E. Evans, C.P.C. Wong, et al., was submitted to Fusion Engineering and Design.

A paper on “DiMES contribution to PMI understanding” by C.P.C. Wong, D.G. Whyte, R. Bastasz, W. Wamplers, J. Brooks, T. E. Evans, W. P. West, J. Whaley, R. Dorner, J. Watkins, L. P. Allain, A. Hassanein, and D. Rudakov, was prepared and presented at the SOFE Conference in October 2003.

10. RF TECHNOLOGY

10.1. COMBLINE ANTENNA

Charles Moeller visited Japan in June 2003 and met with Y. Takase (Univ. of Tokyo) and researchers at NIFS. Considerable work had been done since Dr. Moeller's August 2002 visit. In the August 2002 visit, various tests had been carried out to determine how best to ensure that operation of the LHD combline would be in an even mode. At the June 2003 visit, the current straps and backplanes had been copper plated, the water-cooling tubes had been brazed in, and the molybdenum faraday shield elements and protective limiters had been installed. Extensive measurements made by N. Takeuchi on the amplitude and phase of the current along the radiating elements of the complete real antenna were presented, but the data seemed inconsistent with the sinusoidal profile that would be expected from a single resonance. Dr. Moeller concluded that for the real LHD antenna, of which the modules are tilted with respect to one another, it is essential that the backplanes be tied together electrically at many places in order for the modules to be coupled properly. This is in contrast to the planar prototype and the JFT-2M antenna, which were comprised of backplanes that were all in the same plane. The action item at the end of the visit was for NIFS personnel to connect the backplanes of a few adjacent modules of the LHD antenna and make new measurements.

Charles Moeller visited Japan again in August 2003 and met with Y. Takase (Univ. of Tokyo) and researchers at NIFS. At the beginning of the August visit, only one pair of backplanes had been connected. During the August visit, a better method of joining the modules was developed. Ground planes were installed on either side of an array of four modules so that cavity measurements could be made, rather than having to deal with traveling waves. With the backplanes joined by many low-inductance ribbons, the current-distribution along a strap was measured to be fairly sinusoidal and reduced to zero at the ends, as expected. Measurements made on the four-module array showed the four-even and four-odd resonant modes, as expected, and it was found that by working slightly above the $\pi/2$ point, the undesired odd mode can be avoided.

The next steps are for the NIFS staff to similarly join all the backplanes of the LHD combline and to make traveling wave measurements on the entire antenna. Photographs of an individual module, the 10-module assembly and a schematic showing how the combline antenna would be installed in the LHD are shown in Fig. 16.

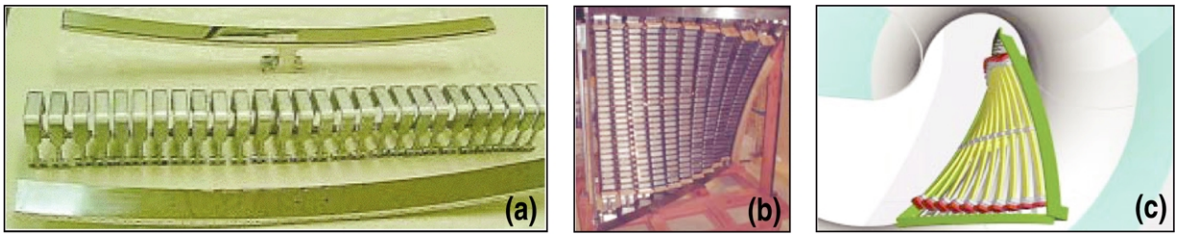

Fig. 16. Combline antenna for use on LHD at NIFS: (a) individual module showing current strap, Faraday shield and back plate, and (b) assembly of 10 modules in a frame, and (c) schematic of future installation in LHD.

10.2. ADVANCED ECH LAUNCHER DEVELOPMENT

As reported previously, GA is developing an advanced mirror under DOE-Advanced Fusion Technology funding. This design uses a copper-plated carbon-fiber composite (CFC) mirror with a high-thermal-conductivity flexible carbon-fiber-bundle heat pipe emanating from the backside of the mirror. A prototype mirror and carbon fiber bundle were fabricated and are awaiting testing in a DIII–D ECH transmission line. Because of higher priority DIII–D ECH tasks, no testing of the CFC mirror was done in FY03. When high-power tests can be performed, they will help determine the suitability of the copper-coated CFC disk as an advanced long pulse launcher mirror. The flexible fiber bundle will also be used with the CFC mirror or with a small metal mirror to demonstrate its ability to remove heat from the mirror to a heat sink.

As reported in the FY02 annual report, Charles Moeller had visited JAERI in August 2002 to participate in low-power testing of JAERI's recently purchased prototype 170 GHz remotely steerable launcher apparatus. The new remotely steerable launcher apparatus at JAERI includes a water-cooled rotating mirror and a 4.6 m long, square cross-section copper waveguide suitable for testing at high power. The inside dimension is 45.7 mm and all four walls are corrugated with a 0.66 mm pitch and with a variation in corrugation depth of $< \pm 0.007$ mm. This apparatus also has the option of inserting four square cross-section miter bends into the line. Low-power measurements without miter bends showed that approximately 95 % of the total radiated power is in the peak at the desired steering angle over the range 0 to ±13 degrees for the electric field either polarized in the plane of steering or perpendicular to the plane of steering. With four miter bends inserted in the line, the losses at >10 degrees were noticeably higher, especially with E in the steering plane. The reason is related to the effect of the corrugations very close to the miter bend mirror. The corrugations on the walls in the plane of the bend near the mirror cannot be perpendicular to both the incident wave and the reflected wave. This has no apparent effect on the HE_{11} mode, but may cause conversion of the higher-order modes present in the tilted beam. Techniques for minimizing this effect are being evaluated.

Prior to visiting JAERI in August 2002, Charles Moeller had designed and fabricated an improved apparatus for measuring the far field radiation pattern from the launcher. The apparatus JAERI had been using allowed for computer-controlled scanning in the x-y plane and also performed the data collection. At each desired steering angle, however, the pickup horn had to be manually adjusted to point to the center of the end of the launcher waveguide. The new scanning apparatus positions the pickup horn on the surface of a sphere so that no manual adjustments are necessary, and the horn is always pointed toward the center of the end of the launcher waveguide. During the first quarter of FY03, various items were loaned to JAERI to enable them to perform very precise measurements of the far field radiation pattern from the launcher apparatus. These items included a log amplifier, an 85 GHz local oscillator, a 170 GHz mixer and low-noise amplifiers. These items enabled JAERI to improve the dynamic range of their measurements from about 10:1 to about 10,000:1. JAERI staff performed measurements over the steering range of 0° to ± 12° and provided the results to GA. The data for positive steering angles were plotted for four different cases: (a) E parallel to the steering direction, no miter bends; (b) E perpendicular to the steering direction, no miter bends; (c) E parallel to the steering direction, four miter bends inserted out of the steering plane; and (d) E perpendicular to the steering direction, four miter bends inserted out of the steering plane. Plots of the results were provided in the FY02 annual report.

Charles Moeller visited JAERI again in June 2003 to participate in short-pulse high-power testing of their 170 GHz remotely steerable launcher apparatus. The plan was to measure thermally the radiation pattern from the launcher and to measure the overall efficiency by attaching a short-pulse calorimeter to the launcher output, set at the anticipated launch angle. Pulses with 550 kW power and 1 ms duration were radiated through a fused quartz window into a fully shielded room toward an Eccosorb screen. The thermal image of the screen was digitally recorded. For steering ranges up to ±12°, there was no power visible other than in the correct direction, and the patterns showed good symmetry. The calorimeter was set up for measurements with E in the plane of steering. The calorimeter was used to measure the power at –5°, 0, +5°, and +10°. The measured power was between 700 and 800 kW, but at –10° and –12° there was as much as 150 kW in the attenuator. The reason for the poor performance at larger angles was found to be that the mirror drive shaft had gradually become unscrewed. The drive mechanism was later repaired and long-pulse high-power tests were resumed in August 2003.

Charles Moeller visited JAERI again in August to participate in long-pulse testing of JAERI's remotely steerable launcher apparatus. Considerable effort was made to set up the Calabazas Creek 1 MW load, including related pre-attenuator and bellows. While Dr. Moeller was visiting NIFS for combline antenna collaboration, JAERI staff performed high-power measurements at 0° with 1 s, 500 kW pulses. With Dr. Moeller's participation, measurements were made at 5°. After he returned to the United States, measurements were

made at 12°. Measurements at 12° initially had a problem with boiling in the pre-attenuator; this was solved by installing a larger pre-attenuator. At 12°, the worst case for losses, the transmission efficiency was found to be 96%, and from thermal imaging, the power dissipated in the launcher waveguide was estimated at 1.8%.

Dr. Moeller modeled the radiation pattern for the 170 GHz remotely steerable launcher apparatus, at 0°, 5°, and 12°. The modeling results were compared with low-power measurements made on the apparatus with H either perpendicular to or in the plane of steering. The agreement between theory and measurements was excellent. As an example, Fig. 17 shows the calculated radiation pattern at a steering angle of –12° (top curve) and the measured patterns for E field in the perpendicular and parallel directions (bottom two curves). The measurements were made using the spherical scanner described above. The agreement between theory and experiment is excellent, especially considering that the "islands" between the peaks at 12° and –12° are 30 dB down from the peak intensity.

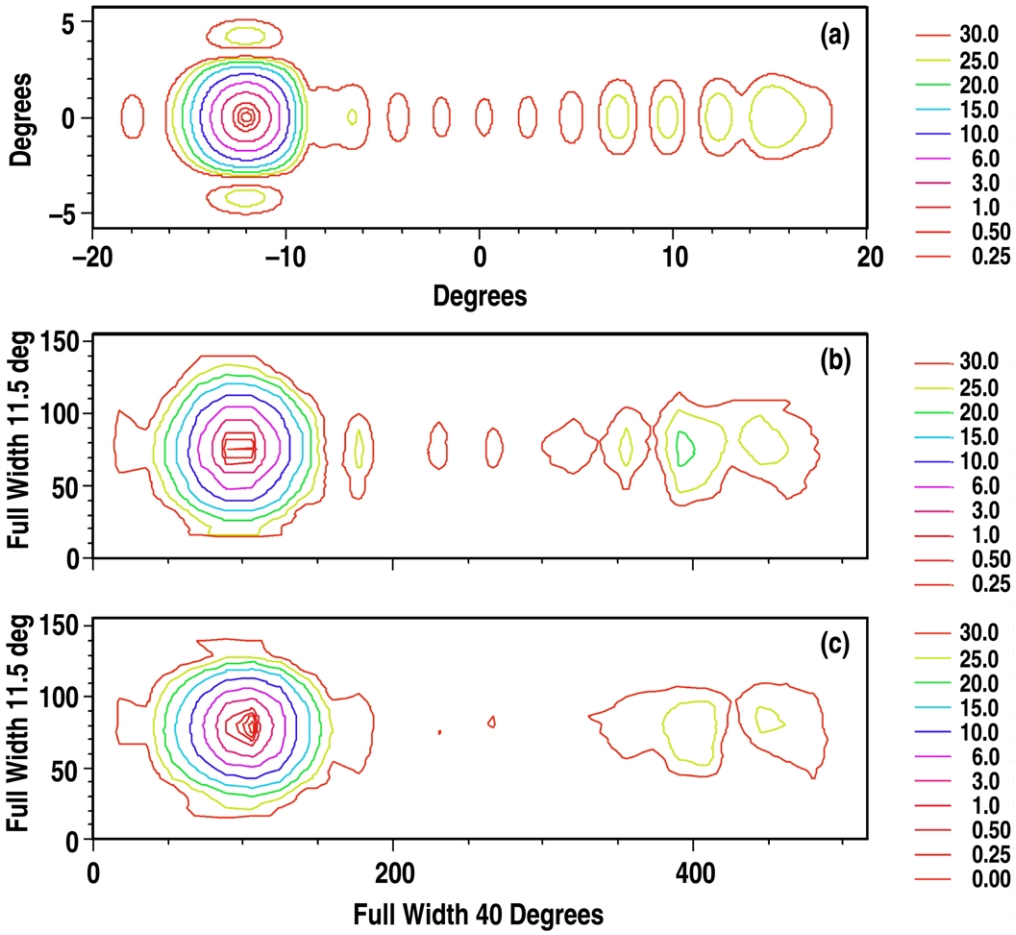

Fig. 17. Calculated radiation pattern at a steering angle of –12° (top curve) and the measured patterns for E field in the perpendicular and parallel directions (bottom two curves).

10.3. WINDOW VALIDATION

A new approach was conceived for measuring the loss tangent of CVD diamond disks. The unique feature of this new approach is that the measurement can be made from one side of the diamond disk, so the technique can be used for measuring the loss tangent on windows after they are mounted on a gyrotron. The new concept is to put a whispering gallery mode cylindrical dielectric resonator made from a low-loss, high-dielectric-constant material, such as silicon, in contact with the part of the diamond surface that is to be measured. The resonator need not be just a right circular cylinder; rather, it can be stepped down in diameter at its ends. These smaller diameter ends then contain an axially evanescent field. The extent of coupling to the diamond substrate can be determined by selecting an appropriate diameter and length of the small diameter ends. If the resonator's relative dielectric constant ε_1' is greater than that of diamond, ε_2', then the field will still be evanescent in the diamond both radially and axially. Therefore, given the typical thickness of the windows, the field in the diamond has no phase shift and there will be a comparable electric field at both of its faces.

Since the resonator does not have any metallic coatings, its unloaded Q is just the $1/\tan(\delta)$ of the dielectric, provided it is made with a high degree of cylindricity. In the case of silicon, $\varepsilon_1' = 11.7$ and $\tan(\delta)$ can be as low as 1×10^{-5}. The corresponding Q is < 1/3 that of the typical confocal resonator, but the volume occupied by the dielectric resonator is comparable to the volume of the diamond it stands on. That suggests that there will be a measurable reduction in resonator Q if $\tan(\delta)$ of the diamond is less than that of the silicon. That would be acceptable for detecting a change in loss after brazing. The reason for requiring $\varepsilon_2' < \varepsilon_1'$ is so that the field in the diamond will be evanescent and energy will not propagate away radially, thereby making $\tan(\delta)$ appear higher than it really is. This resonator also has the inherent advantage of excellent mechanical stability, while its temperature can be controlled by regulating the window temperature.

The (n,0,0) whispering gallery modes will have much higher Qs than lower-order modes, and are separated from each other by several gigahertz, so a rather simple excitation scheme can be used. The angular mode number need not be extremely high. It only has to be large enough so that the cylinder can be made precisely. For example, there is a reference in the literature to a plane alumina resonator 5 mm in diameter and 0.635 mm high (no diameter steps at the ends) having $E_{14,0,0}$ and $H_{14,0,0}$ resonances near 110 GHz. The resonator can also be designed for 170 GHz or other frequencies. A hollow cylinder can be used to discriminate against the (n,1,0) modes, which seem to be the other high Q competing modes. It is also possible to selectively excite the desired mode. This can be done by means of a coupled cavity resonator, similar to the TE22,6 mode generator made by GA, but with an evanescent output.

During the year, a method was conceived for measuring loss tangents of diamond disks mounted in waveguide vacuum window assemblies. The measurement of loss tangent can be

performed by placing the assembly in a corrugated waveguide cavity. To prevent mode competition from obscuring the measurement, the partially transmitting mirrors at each end of the cavity can be placed at the ends of transitions from small rectangular waveguide to the HE_{11} mode in corrugated waveguide. To minimize diffraction loss at the diamond, corrugated waveguide HE_{11}/HE_{12} mode mixture generators can be placed in the cavity on either side of the window assembly. If the diamond disk is located midway between the two mirrors, then in a frequency scan the resonances will alternate between high and low loss. The loss tangent can be determined from the difference in these losses, or by comparison with a window assembly without the diamond. Tracking-circuits or possibly a lock-in amplifier allow rapid frequency scans that avoid the need for special thermal stabilization of the cavity, while maintaining high signal-to-noise ratio. The waveguide parts and mode mixture generators for these loss tangent measurements have not yet been fabricated, pending the availability of sufficient funds to purchase the parts, assemble the apparatus, and perform measurements on a sample CVD diamond disk.

10.4. INTERNATIONAL COLLABORATION

A joint U.S.-Japan, EU-Japan, U.S.-EU workshop on RF Technology was conducted February 12–14, 2003 at Marina Del Rey, California. This was the first such meeting with the United States and EU having a formal bilateral exchange in this area. There were 35 attendees at the meeting: seven from Japan, 10 from Europe, and the rest were from the United States. Presentations were given covering ICRH, ECH, and LHH technologies. The contributions included talks on mode conversion, antenna matching, and recent developments on 170 GHz gyrotrons and transmission line systems.

Plans were made for U.S. delegation participation in the joint U.S./Japan/EU RF Technology Exchange held at Tokai, Japan on September 25–26, 2003, just prior to the IRMMW 2003 conference. JAERI was the host for this joint workshop. R. Olstad gave a presentation on “Recent Results on DIII–D ECH and Other RF Programs at General Atomics.” C. Moeller gave a presentation on “Recent Results of Measurements on a Remote Steering Launcher for 170 GHz.” D. Remsen presented a paper for M. Shapiro (MIT) on “Experimental Research on High Efficiency 1.5 MW 110 GHz gyrotron.” The U.S. participants were from GA, ORNL, and PPPL. The Japanese participants were from JAERI, NIFS, Tsukuba Univ., Kyoto Univ., Ibaraki Univ. and Kyushu University. The EU participants were from Univ. of Stuttgart, FZK, CIEMAT and FOM. In addition, two observers from Korea attended the meeting and gave presentations on KSTAR status.

At the conclusion of the meeting, a list of proposed U.S./Japan, U.S./EU and Japan/EU collaborations was prepared. One of main areas of interest for collaboration among the parties is in the area of remotely steerable launchers for ITER.

At the workshop there was some discussion on where the next U.S./Japan and U.S./EU meetings will be held. The Japanese university staff are presently unable to travel to Europe. As a result, the tentative plan is for the next EU/U.S. RF exchange meeting to be held in The Netherlands on October 4–5, 2004, following the SOFT and IRMMW 2004 meetings in Venice and Karlsruhe, respectively. If the Japanese university contingent cannot attend the meeting in the Netherlands, the plan is either to hold a separate U.S./Japan meeting in the United States during CY04 or have JAERI, but not Japanese university, participation in the exchange meeting in The Netherlands.

10.5. CONFERENCES/MEETINGS

Joint U.S.-Japan, EU-Japan, U.S.-EU workshop on RF Technology (22nd U.S.-Japan RF Exchange) February 12–14, 2003 at Marina Del Rey, California.

Joint U.S./Japan/EU RF Technology Exchange (23rd US-Japan RF Exchange) held at Tokai, Japan on September 25–26, 2003.

10.6. PUBLICATIONS

K. Takahashi, C.P. Moeller, et al., Fusion Engineering and Design **65**, 589 (2003).

11. REFERENCES

[1] Callahan-Miller, D.A., and M. Tabak, Phys. Plasmas **7**, 2083 (2000).

[2] Latkowski, Jeff, "Heavy Ion Fusion Target Workshop," General Atomics, April 22, 1999.

[3] Moir, Ralph, "Flibe Coolant Cleanup and Processing in the HYLIFE-II Inertial Fusion Energy Power Plant," Lawrence Livermore National Laboratory Report UCRL-ID-143228 (2001).

[4] C.B. Baxi, et al., "Thermal Stress Analysis of FIRE Divertor," Fusion Engineering and Design **66–68**, 323 (2003).

[5] M. Ulrickson, private communication, Sandia National Laboratory, Albuquerque, New Mexico, March 2003.

ACKNOWLEDGMENT

This report was prepared for the U.S. Department of Energy under Contract No. DE-AC03-98ER54411.